Journal Name

ARTICLE TYPE

Cite this: DOI: 10.1039/xxxxxxxxxx

Relaxation dynamics of ^{3}He and ^{4}He clusters and droplets studied by near infrared and visible fluorescence excitation spectroscopy

Klaus von Haeften,*[†a] Tim Laarmann,[†] Hubertus Wabnitz,[†] and Thomas Möller[†b]

Received Date
Accepted Date

DOI: 10.1039/xxxxxxxxxx

www.rsc.org/journalname

The relaxation dynamics of electronically excited ^{3}He and ^{4}He clusters and droplets is investigated using time-correlated near-infrared and visible (NIR/VIS) fluorescence excitation spectroscopy. A rich data set spanning a wide range of cluster and droplet sizes is produced. The spectral features broadly follow the vacuum ultraviolet excitation (VUV) spectra. However, when the NIR/VIS spectra are normalised to the VUV fluorescence, regions with distinctly different cluster size and isotope dependence are identified, enabling deeper insight into the relaxation mechanism. Particle density, location of atomic-like states and their principal quantum number, n, are found to play an important role in the relaxation. For states with $n = 3$ and higher, energy only within the surface region is transferred to excited atoms that are subsequently ejected from the surface and fluoresce in vacuum. For states with $n = 2$, energy from the entire region within clusters and droplets is transferred to the surface, leading to the ejection of excited atoms and excimers. Here, the energy is transferred by excitation hopping, which competes with radiative and non-radiative decay, making ejection and NIR/VIS fluorescence inefficient in increasingly larger droplets.

1 Introduction

The prospect of investigating geometrically confined quantum fluids, free from external interactions in vacuum using helium cluster and droplet beams, has excited scientists across disciplines for almost half a century[1,2]. The research activity and continued interest in this topic within the scientific community is reflected by numerous review articles[3–13]. The research addresses intrinsic properties of helium clusters, including the highly quantum nature of helium-complexes[14,15], as well as applications in nanoscience, exploiting specific features of helium droplets. The latter include the pick-up technique to isolate single atoms or molecules ultra cold and liquid matrix on a nanoscale,[16] or to assemble molecular complexes or clusters, taking advantage of the weak-interaction and superfluid nature of ^{4}He droplets[17–19]. These features have enabled the fabrication and the study of metal clusters with good control of their size and temperature, which in helium droplets is much lower than what can be achieved for free metal clusters in beams[20–25]. Very recently, the pick-up technique had been extended to produce metal clusters and nanoparticles using ionic helium droplets[26,27]. Profound insight into molecular quantum level structure and molecular dynamics in superfluids has been obtained using traditional infrared laser spectroscopy in the frequency domain[28–32] as well as in the time domain, using rotational coherence spectroscopy[33,34]. Comparative experimental studies between clusters of the stable isotopes ^{3}He and ^{4}He aiming at elucidating effects of superfluidity have been performed, although these attempts remain rare given the effort required to cope with only very limited quantities of the expensive ^{3}He gas during the experiments[35–40].

This paper deals with the relaxation dynamics of electronically excited ^{3}He and ^{4}He clusters and droplets[41–49]. It builds strongly on previous work on electronically excited bulk liquid and the use of fluorescence spectroscopy for detection[50–64]. The topic of electronically excited helium clusters has also been addressed by theory[65–72].

Previous studies of electronically excited ^{4}He clusters established the presence of perturbed atomic-like states related to the $2p^1P \leftarrow 1s^1S$ and dipole-forbidden $2s^1S \leftarrow 1s^1S$ transitions of helium atoms[41]. Similar features are observed in bulk liquid helium[52]. Comparison between ^{3}He and ^{4}He clusters and droplets showed that the magnitude of the perturbation is controlled by the particle density[37]. A comprehensive study spanning a wide range of cluster and droplet sizes revealed the location of higher electronically excited features at the surface of helium clusters and droplets[39]. In very small ^{4}He clusters, the radius of the electronically excited orbitals is larger than that of the clusters. These states can be understood as a Rydberg electron orbiting around a positively charged cluster[73–75].

* corresponding author; E-mail: klaus.von.haeften@rub.de
† DESY, Notkestr. 85, 22607 Hamburg, Germany
[a] present Address, Kanano GmbH, Sedanstr. 14, 89077 Ulm, Germany.
[b] present Address, Institut für Optik und Atomare Physik, Technische Universität Berlin, Hardenbergstr. 36, 10623 Berlin, Germany.

After electronic excitation, the energy localises in electronically excited atomic and molecular states[76], very similar to electronically excited bulk liquid helium[53–55]. Depending on the cluster size, this happens preferentially at the surface, leading to fast ejection of excited atoms and molecules[46,47,76] or, in the case of very large droplets, in the bulk volume where spherically symmetric excitations form bubbles wherein the electronically excited helium excimers are confined[38].

Detailed information about the timescales between electronic excitation of helium droplets and the ejection of excited atoms and molecules has been obtained using pump-probe experiments[44,46,47,77,78] and ion detection[10]. These experiments confirmed the overall picture of the localisation of energy in singlet and triplet atomic and excimer states and the relevance of fast ejection of atomic and molecular species[49].

To date, our picture of the relaxation dynamics in helium clusters and droplets remains nevertheless incomplete because the energy ranges and size ranges covered in the research so far are rather limited. To fill this gap and work towards a comprehensive understanding of the relaxation dynamics in helium clusters and droplets, we present new spectroscopic data, spanning a wide range of excitation energies and cluster sizes, including both stable isotopes ^{3}He and ^{4}He.

Complementary to our previous work[39], the fluorescence excitation spectra of clusters and droplets presented here cover the same broad range of sizes, but are recorded with detectors sensitive to the near-infrared and visible (NIR/VIS) spectral ranges. Such spectra are indicative of the fluorescence emitted from ejected atoms and molecules following electronic excitation of the clusters and droplets. By normalising these spectral data with the corresponding VUV fluorescence excitation spectra reported earlier[39], it is possible to deduce the efficiency of energy localisation at the surface and subsequent ejection of excited species. Examination of the cluster size dependence and time-correlation of the detector signals help to identify states correlated with the atomic 2p levels, where excitations are found to hop between neighbouring atoms, localise and eventually reach the surface. There, excited atoms or excimers are ejected, emitting NIR/VIS fluorescence in great distance of the surface in vacuum. States correlated with the atomic 2s levels do not show this behaviour. Instead, VUV fluorescence to the ground state or ejection of meta stable atoms are the preferred relaxation channels. For levels at higher energy, the location of the excitations in the surface region and the wider reach of the excited wavefunctions towards the centre determine the relaxation. We identify energy bands where immediate ejection dominates, whereas in other bands non-radiative decay into lower-lying excited states prevails.

2 Experiment

The experiments were performed at the permanent experimental station *CLULU* at beam-line *I* at the former DORIS III positron storage ring at DESY in Hamburg.

^{3}He and ^{4}He clusters and droplets were produced in an ultra-high-vacuum molecular beam apparatus by supersonic expansion of 6.0 helium gas at stagnation pressures of $p_0 = 40$ bar for ^{4}He and $p_0 = 7$ bar for ^{3}He through an orifice of 5 μm in diameter into the vacuum. Due to the high costs, ^{3}He gas was recycled throughout experimental runs and stored in a gas cylinder for future experiments. The maximum gas pressure delivered by the compressor used in the recycling apparatus was 7 bar. Further details are available in the literature[73,79]. In other experiments, different orifice diameters were used with very good results for 20 μm orifice diameter[79]. The data presented here have throughout been recorded using a 5 μm orifice with the objective to facilitate assignment of the cluster and droplet size, taking benchmark size measurements reported by Harms et al. as reference[80], who operated their apparatus using a 5 μm orifice. However, the different stagnation pressures used represented an obstacle to the interpretation of the data. Harms et al. used 10, 20 and 25 bar, whereas here 7 bar was used because of the limited maximum pressure of the membrane compressor used in the recycling apparatus[80]. As the cluster size is a central issue in this paper and the relation between orifice temperature T_0 and the average number N of atoms in a cluster or droplet has been investigated thoroughly in specific size ranges only, T_0 is indicated for every spectrum. We note that for a given average number of atoms, N , the average half-width of the size distribution is roughly N as well.

The helium cluster and droplet beam was directed into the focal spot of the monochromatic synchrotron light beam using a x-y-z manipulator to maximise fluorescence yield by adjusting the overlap of the cluster beam with the synchrotron light. To achieve maximum cluster and droplet density in the focal spot, the option of using a skimmer was abandoned. The distance between focus and orifice was about 3 mm, taking into account that the focal region extended from 0.5 mm after the nozzle to 5.5 mm downstream. Likewise, stray light emerging from light scattered off the cluster source was minimised to reach a good compromise in signal-to-noise ratio. Further details are reported in the literature[39].

Synchrotron radiation emitted from a bending dipole magnet was deflected upwards, leading vacuum ultra-violet synchrotron radiation via mirrors to two experimental stations, which shared a 15^0-normal-incidence McPherson monochromator. Details of the experimental set-up comprising of the molecular beam apparatus *CLULU* and the differentially pumped beam-line are provided in the literature[81].

The fluorescence intensity was recorded using the time-correlated photon counting technique, taking advantage of the specific time-structure of the synchrotron light pulses emitted from discrete positron bunches. Short-lived fluorescence is indicative of non-radiative decay, operating in parallel to fluorescence decay, whereas long-lived fluorescence is indicative of the absence of such competing decay channels.

In addition, different detectors sensitive to specific spectral wavelength ranges were used. VUV fluorescence was recorded using a thin plate coated with a film of sodium salicylate before a window in vacuum and a XP 2020 photomultiplier (*Valvo/Philips*) outside in air. With this arrangement, VUV photons were converted to the spectral sensitivity range of the photomultiplier. Previous experiments established that visible photons emitted from the helium clusters were not detected, thus excluding

double-counting and cross-detection[73]. The number of absorbed photons is to, a very good approximation, proportional to the number of detected VUV photons[73,81]. There are only few limitations such as auto-ionisation above 23 eV or annihilation for very large droplets. In large droplets, more than one excitation per synchrotron light pulse may occur[73,82].

Fluorescence emitted in the visible and near-infrared spectral ranges (NIR/VIS) was guided via a lens system to a R 943 detector (*Hamamatsu*), a feature of the experimental apparatus that is central to the present paper. This detector was insensitive to VUV photons. Consequently, it was possible to investigate dynamic processes after electronic excitation of the clusters and droplets, which lead to fluorescence in the NIR/VIS ranges. This NIR/VIS fluorescence is due to transitions to excited levels that are lower in energy[76]. In some cases, energy is transferred to states from which transition to the ground state is forbidden and consequently, the NIR/VIS fluorescence can become rather intense[83].

Time-resolved excitation spectra were recorded by counting photons selectively in different, specific channels, taking advantage of the pulsed nature of synchrotron radiation. The pulses generated from each detected photon by the photo multipliers were counted in their entirety in a counter for the *integral* fluorescence. In addition, the signal was split into two further channels, which were gated using Time-To-Amplitude (TAC) converters and Constant-Fraction-Discrimination, providing a method to count photons only during dedicated time-windows. For both VUV and NIR/VIS detection a time window of 3 to 18 ns after the excitation pulse was set to measure short-lived fluorescence and a time-window of 40 to 172 ns was set to record long-lived fluorescence.

The sensitivity of the NIR/VIS channel was calibrated against the VUV channel using the known ratio of the Einstein-coefficients of emission A for the $3p^1P \rightarrow 2s^1S$ and $3p^1P \rightarrow 1s^1S$ transitions[84]. The calibration was performed using an atomic helium beam when the cluster source was at room temperature and cluster formation could be safely excluded. Following this procedure, the count rate of the R 943 detector was multiplied with a calibration factor of 0.45 whenever the fluorescence of the two different wavelength ranges was compared.

Otherwise, the experimental data presented in the this paper were acquired during the same experimental run and therefore under identical conditions as outlined in[39], notably at a constant photon flux (in eV bandwidth intervals) and a resolution of 26 meV (using 100 μm-wide entrance and exit slits). All other calibration procedures were identical.

3 Results

3.1 Cluster and droplet-size dependence

In the following, excitation spectra of the fluorescence emitted in the NIR/VIS spectral range of ^{4}He clusters and droplets are shown. Fig. 1 to Fig. 3 are organised in a sequence from high to low cluster source temperatures, corresponding to average cluster sizes from N = 80 atoms to 10^5 atoms. The presentation follows the sequence of figures in our previous publication[39].

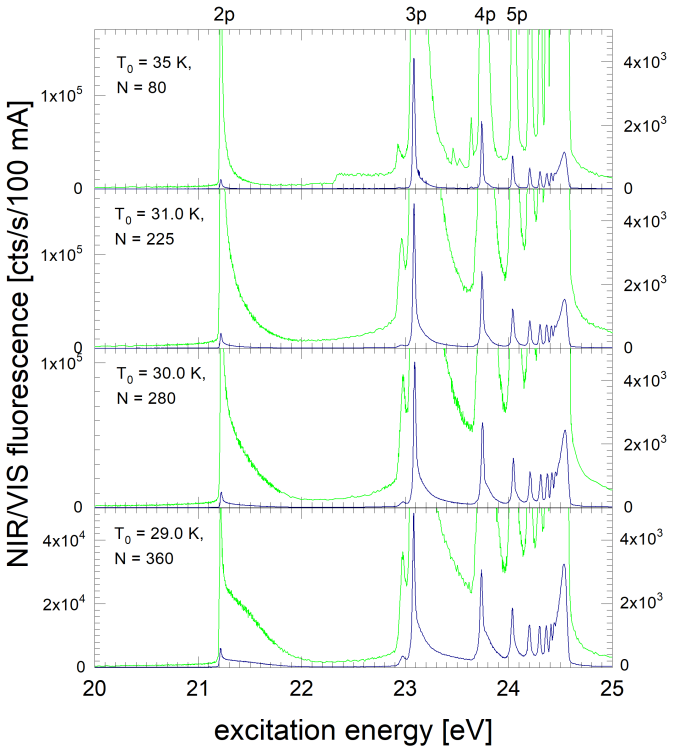

Fig. 1 Excitation spectrum of the NIR/VIS fluorescence emitted from small ^{4}He clusters (x 10 in light green, scale on right). The N = 80 spectrum on the top is affected by artefacts between 22.5 and 22.9 eV and between 23.2 and 23.7 eV. The stagnation pressure for all experiments with ^{4}He was p_0 = 40 bar.

In Fig. 1, the NIR/VIS excitation spectrum is dominated by sharp peaks at the position of the transition to the np^1P atomic levels of helium. To reveal finer details, a tenfold enhanced spectrum is shown as well (in light-green, scale on right). In the enhanced spectrum, it can be observed that there are also sharp peaks close to the atomic $3s^1S$ level and also a shoulder close to the atomic $4s^1S$ levels (the energies of the singlet s levels are indicated in Fig 6). Furthermore, the sharp peaks are accompanied by smoothly decaying wings on the high-energy sides. The spectrum of N = 360 shows a bump at 21.5 eV, indicating that the wing starts to evolve into a band. In summary, the features are very similar to the excitation spectrum of the VUV fluorescence presented earlier[39] with the exception that the features close to the atomic $2p^1P$ level are much less intense than their counterparts seen in the VUV fluorescence excitation spectrum.

Fig. 2 shows the NIR/VIS excitation spectrum of increasingly larger ^{4}He clusters between N = 450 and N = 1800 atoms. With increasing size, the bump at 21.5 eV in Fig. 1 evolves into a distinct band when the average cluster size reaches N = 1000 and beyond. Above 23 eV, the wings close the gap between the np^1P ($n > 2$) atomic levels. When the cluster size approaches N = 1000, the wings merge to a continuous band which extends up to the ionisation threshold of helium atoms at 24.56 eV. Different to the VUV fluorescence excitation spectra presented earlier[39] there is almost no NIR/VIS fluorescence beyond 24.56 eV.

Fig. 3 shows the NIR/VIS excitation spectrum of very large clus-

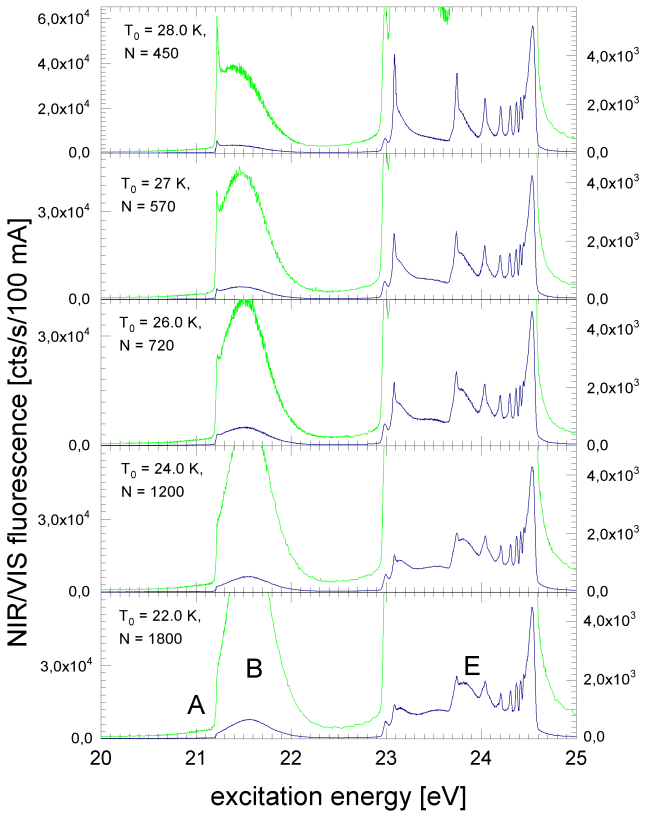

Fig. 2 Excitation spectrum of the NIR/VIS fluorescence emitted from medium-sized ^{4}He clusters. The wings merge into broader features. At 21,5 eV a distinct, Gaussian shaped feature emerges, labelled *Band B* in earlier publications.

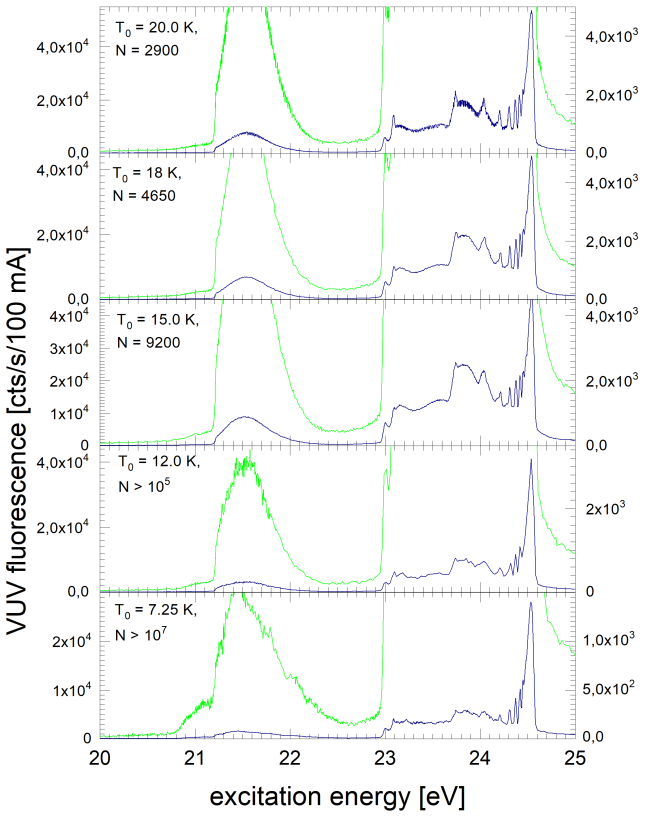

Fig. 3 NIR/VIS excitation spectrum of very large clusters and droplets. At cluster source temperatures below 15 K, the cluster growth process changes. Here, helium cools during the expansion below the phase transition temperature and large droplets are formed by fragmentation of liquid helium. The corresponding spectra are characterised by artefacts due to multiple photon absorption and absorption saturation effects.

ters and droplets, corroborating the trends observed in Fig. 1 and Fig 2. Below $T_0 = 15$ K, the spectral features are distorted. This can be attributed to a number of artefacts that are related to the photo-excitation of large droplets such as saturation, multiple photon absorption and light scattering[81]. Artefacts are also observed in the VUV fluorescent excitation spectra presented earlier[39].

In summary, the NIR/VIS excitation spectrum of ^{4}He clusters and droplets largely follows the VUV fluorescence excitation and the photo-absorption, respectively. However, it should be noted that in the region below the $2p^1P \leftarrow 1s^1S$ transition of helium atoms at 21.2 eV no intensity is observed, despite the fact that the VUV fluorescence excitation spectrum is showing a distinct band, labelled *A* in earlier publications[37,39,41]. Also, the VUV fluorescence excitation spectrum shows intensity above the ionisation threshold of helium atoms at 24.56 eV when the clusters and droplets become very large[73]. In this region, NIR/VIS fluorescence is practically absent.

3.2 Isotope dependence

In Fig. 4 and Fig. 5, NIR/VIS fluorescence excitation spectra of ^{3}He droplets are shown. ^{3}He does not form bound states in dimers or small clusters. Calculations show that clusters smaller than 26 atoms are unstable[85]. Also, beams of ^{3}He droplets are formed by fragmentation of liquid ^{3}He during expansion of ^{3}He gas. As a consequence, the size distribution of the droplets in the beams is entirely different from ^{4}He and characterised by the absence of small clusters[86]. Previous measurement of ^{3}He droplet sizes using the cross-beam-deflection method showed a sharp on-set of droplet formation at a certain temperature is observed. With decreasing temperature, the average droplet sizes were found to decrease slightly[86]. Here, we take these size measurements as a benchmark, however, we note that the beam length of the apparatus used in[86] was about 100 times longer. Also, the stagnation pressures p_0 differed. The membrane compressor could not deliver stagnation pressures higher than $p_0 = 7$ bar, compared to Harms et al. who were using 10, 20 and

25 bar, respectively. Thanks to the stagnation pressure dependence, observed in[86], it was possible to extrapolate some droplet sizes that would be expected at p_0 = 7 bar. Because of these circumstances, the peculiar droplet formation for ^3He_n and ongoing fragmentation of droplets along their journey towards the detector, we have to take uncertainties in the stated sizes of the ^{3}He droplets into account. The orifice temperature indicated in Fig. 4 and Fig. 5 serves as an additional reference to assess droplet size trends and as a guide for discussion.

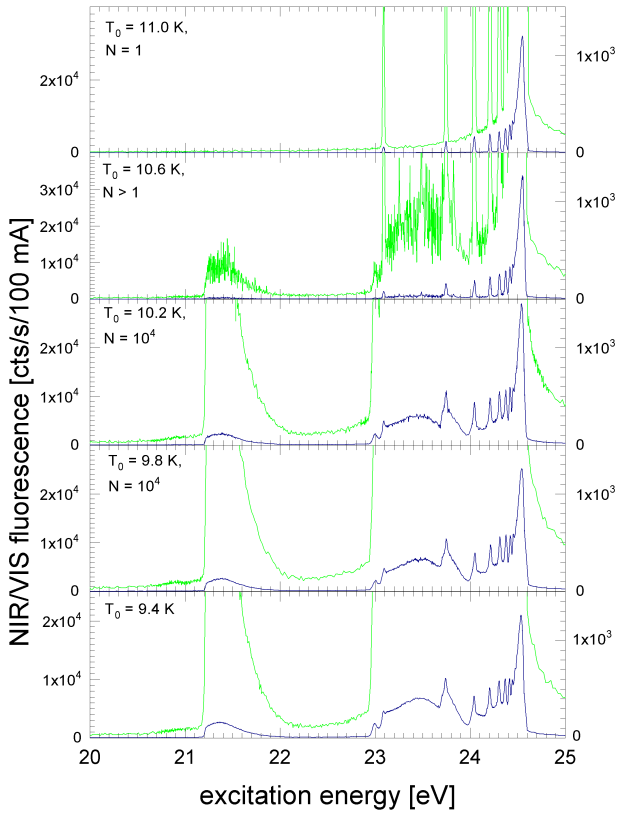

Fig. 4 NIR/VIS fluorescence excitation spectra of ^{3}He. At orifice temperatures of T_0 = 11 K, only ^{3}He atoms are excited. At T_0 = 10.6 K increased noise indicates that droplets of ^{3}He begin to form. For lower orifice temperatures the spectral features of ^{3}He droplets are fully evolved. The stagnation pressure for all experiments with ^{3}He was p_0 = 7 bar.

In Fig. 4, the NIR/VIS excitation of ^{3}He droplets is shown. At a source temperature of T_0 = 11K, only peaks at energies of the dipole-allowed $np^1P \leftarrow 1s^1S$ transitions are observed, indicating that only atoms are in the beam. An exception is the $2p^1P \leftarrow 1s^1S$ transition energy where hardly any intensity is measured in the NIR/VIS detection channel. After population of the $2p^1P$ state two fluorescent decays are possible: (i) to the ground state, producing VUV fluorescence and (ii) to the slightly lower lying $2s^1S$ level, producing fluorescence in the NIR. The intensity of the $2p^1P \leftarrow 1s^1S$ transition is so small because the Einstein coefficient of emission of the $2p^1P \rightarrow 2s^1S$ transition ($A_{2p,2s}$ = 1.9746×10^6 s^{-1},[87]) is much smaller than that of the $2p^1P \rightarrow 1s^1S$ transition ($A_{2p,1s}$ = 1.7989×10^9 s^{-1},[87]), the ratio between the two scaling with the third power of the transition energy.

In this respect, we emphasise that for very small ^{4}He clusters the situation is different. While the shape of the spectral features around 21.2 eV are not much different from atoms, the comparatively high intensity in the NIR/VIS region seen in the spectra of ^4He_n clearly indicates that the fluorescence must be due to small clusters (compare with Fig 1). Hence, the absence of any NIR fluorescence at 21.2 eV is strong evidence for the purity of the ^{3}He atomic beam, i.e. the complete absence of clusters, including the smallest clusters.

For higher energies, the NIR/VIS fluorescence intensity of the excited np^1P levels increases progressively. This observation is expected because of the increasing lifetime of Rydberg states and the associated change of the VUV – NIR/VIS fluorescence branching ratios. With increasing principal quantum number, the Einstein-coefficient of transitions to the ground state decreases. As a consequence, the transitions to the lower lying excited s and d states, which fluoresce in the NIR/VIS spectral ranges and compete with the VUV fluorescence, are progressively favoured.

Furthermore, Fig. 4 shows the onset of droplet-related fluorescence at source temperatures of T_0 = 10.6 K. At T_0 = 10.2 K, the NIR/VIS fluorescence excitation spectrum is fully evolved, showing features typical for large droplets and similar to those of large ^{4}He droplets. The rather abrupt appearance of ^{3}He droplets within a relatively small range of the source temperature of less than 0.8 K corroborates the peculiar droplet formation characteristics of ^{3}He which are fundamentally different from their bosonic ^{4}He counterpart.

Fig. 5 shows that this trend is unchanged when the source temperature decreases further. The extrapolated droplet size of around N = 10^4 remained broadly constant. Again, this can be attributed to the specific formation process of ^{3}He droplets by fragmentation and the entire absence of small clusters due to the lack of bound states. Below T_0 = 9.0 K, extrapolation was not possible, but the data reported by Harms et al. suggest that size begin to increase strongly[86].

The intensity of the NIR/VIS fluorescence excitation bands of droplets exceed the NIR/VIS fluorescence intensity of atoms. With decreasing source temperature, the intensity at the energies np^1P increases and remains at its maximum value at T_0 = 9.4 K to 8.0 K.

3.3 Introduction into normalisation of NIR/VIS fluorescence excitation spectra

Fig. 1 to Fig. 5 show that there are distinct differences between the NIR/VIS and VUV fluorescence excitation spectra, such as the absence of band A and the rather weak NIR/VIS intensity above the ionisation threshold. Otherwise, the spectral features of the NIR/VIS fluorescence excitation spectra appear rather similar to those of their VUV fluorescence excitation spectra counterparts[39], particularly their overall shape.

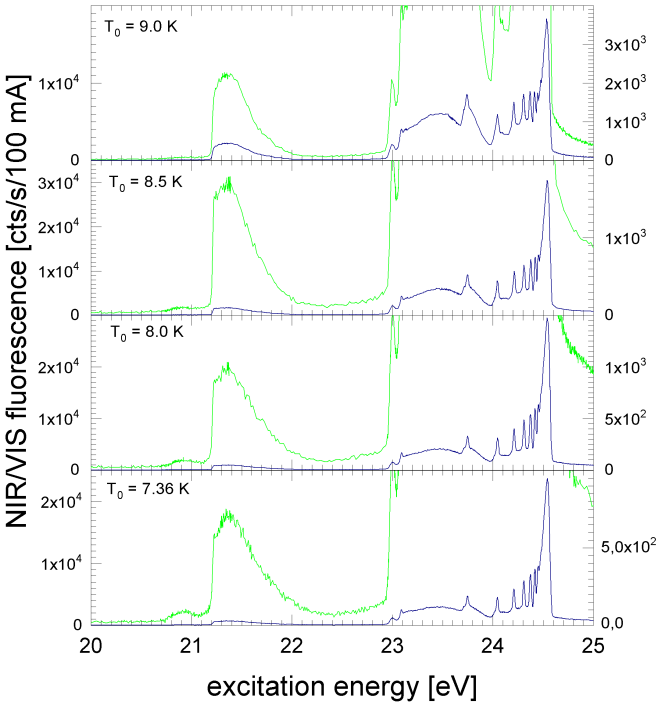

Fig. 5 NIR/VIS fluorescence excitation spectra of large ^{3}He droplets produced at orifice temperatures between 9.0 K and 7.4 K. The overall shape of the spectral features shows little change. However, the overall intensity decreases with decreasing orifice temperature. Note the varying intensity scale.

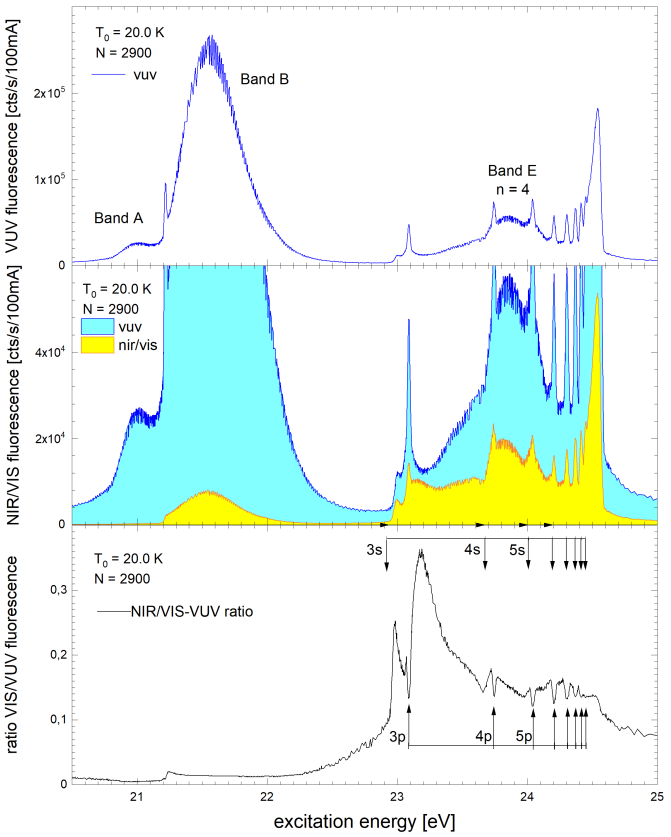

Fig. 6 Example how normalised fluorescence excitation spectra of He clusters and droplets are produced. Top panel: VUV spectrum (as published earlier in[39]). Middle panel: NIR/VIS (yellow) and VUV spectrum (blue). Bottom panel: NIR/VIS normalised by VUV spectrum (calibrated, see text). The bands are labelled in line with the literature ([41]). The energies of the atomic s and p singlet resonances are indicated by vertical arrows[88].

Closer inspection of the intensities, however, reveals more subtle differences between NIR/VIS and VUV fluorescence excitation spectra. These differences are nevertheless significant. They distinctly depend on the cluster and droplet sizes as will be shown below.

To visualise and interpret these differences, it is helpful to normalise the excitation spectra of the NIR/VIS fluorescence to the VUV fluorescence. The VUV fluorescence excitation spectra of helium clusters and droplets are to a good approximation proportional to the photo absorption[39]. Therefore, the normalised spectra represent quantum efficiencies of NIR/VIS fluorescence and also of the ejection of excited atoms and excimers, the underlying process that is associated with NIR/VIS fluorescence.

Fig. 6 shows how the normalised spectra are generated. In the top panel, the VUV fluorescence excitation spectrum of ^{4}He droplets of size N = 2900 atoms are shown. We note that this spectrum, and all other VUV fluorescence spectral data required for the normalisation, has been reported earlier[39]. In the middle panel of Fig. 6, VUV and NIR/VIS features are shown alongside for comparison. It is apparent that the shapes of the features in both spectra are very similar, however, the intensity of the NIR/VIS fluorescence spectra is always lower than the VUV fluorescence.

In the bottom panel of Fig. 6, the normalised NIR/VIS spectrum is shown. The normalised spectrum is produced by division of the NIR/VIS spectrum by the VUV spectrum multiplied by a calibration factor to take account for the different sensitivities of the detectors, as mentioned above.

We will see below that for the understanding of relaxation dynamics normalisation is very helpful, providing a more meaningful presentation of spectral data. For example, normalised NIR/VIS fluorescence excitation spectra can reveal sharp peaks close to the position of dipole-forbidden atomic transition energies that are very difficult to spot otherwise[83]. In the sections below, we will therefore show normalised spectral data of the integral, short-lived and long-lived NIR/VIS fluorescence alongside charts that investigate the cluster size dependence. The labels shown in Fig. 6 indicate the location of reference energies of specific interest, such as *Band A, B* and *E* and the atomic singlet s and p energies of helium.

3.4 Normalised integral, short-lived and long-lived NIR/VIS spectra of ^{4}He$_n$

Normalised NIR/VIS spectra of ^{4}He$_n$ clusters are shown in Fig. 7, 8 and 9. The normalised spectra of the entire NIR/VIS fluorescence (filled squares, blue colour) are shown alongside spectra recorded in short (filled circles, red colour) and long (filled triangles, green colour) time windows after the excitation light pulses.

The normalised NIR/VIS spectrum of small ^{4}He clusters is char-

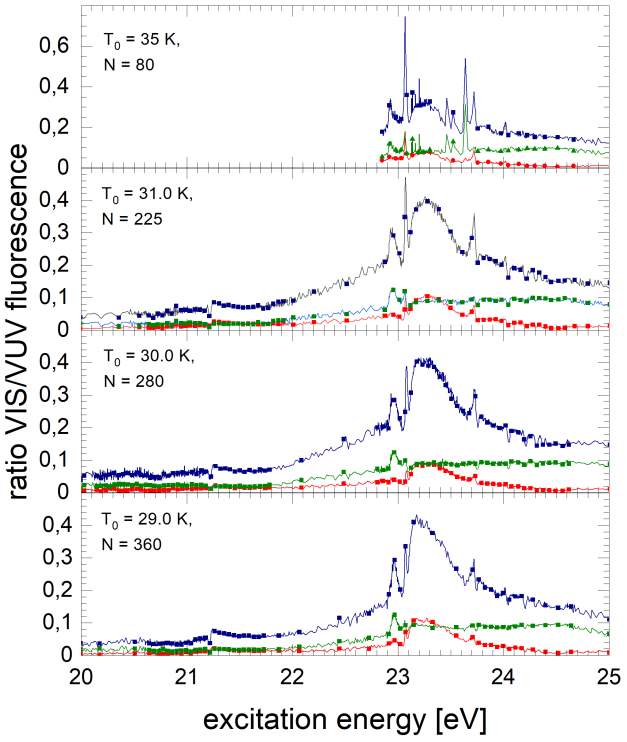

Fig. 7 Normalised NIR/VIS spectra of small ^4He_n clusters. The spectrum of N = 80 clusters at the very top is unfortunately affected by artefacts between 22.5 and 22.9 eV (not shown) and between 23.2 and 23.7 eV. The total NIR/VIS fluorescence is shown in blue colour with filled square symbols, whereas the NIR/VIS fluorescence in the short time window is shown in red with filled circles and the NIR/VIS fluorescence in the long time window is shown in green with filled triangles. This colour and symbol code is kept consistently in this paper.

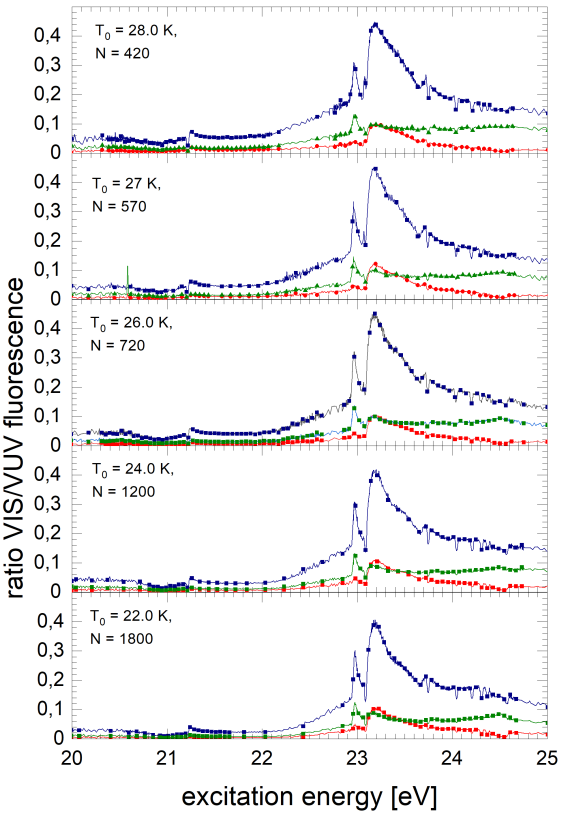

Fig. 8 Normalised NIR/VIS fluorescence spectra of medium-sized ^4He_n clusters (blue filled squares). Short-lived normalised NIR/VIS fluorescence spectra are shown in red with filled circles and long-lived in green, with filled triangles.

acterised by very sharp and very intense peaks close to the positions of the atomic $3s^1S \leftarrow 1s^1S$ and $3d^1D \leftarrow 1s^1S$ transitions. These peaks reach up to 75 % of the normalised NIR/VIS intensity. In other words, out of four emitted VUV photons (transitions to the ground state), three photons are emitted due to transitions into lower lying electronically excited states. In addition, peaks are identified close to the atomic $4s^1S \leftarrow 1s^1S$, $5s^1S \leftarrow 1s^1S$ and $6s^1S \leftarrow 1s^1S$ transition energies – transitions that are all dipole-forbidden for helium atoms. The $3s^1S \leftarrow 1s^1S$ resonance and these higher energy peaks are all slightly blue-shifted with respect to the atomic transition energy. The peak at the $3d^1D \leftarrow 1s^1S$ energy does not show any appreciable blue-shift. The blue shift will be discussed in a separate section below.

The sharp features at the position of the atomic transitions are also visible in the short-lived and long-lived correlated NIR/VIS fluorescence excitation spectra, showing an interesting intensity pattern: The $3s^1S \leftarrow 1s^1S$ related feature is favoured in the long-lived correlated spectrum, whereas the $3d^1D \leftarrow 1s^1S$ related feature is more short-lived; likewise the $4s^1S \leftarrow 1s^1S$-related transition shows higher intensity in the long-lived-correlated spectrum. Furthermore, the $3d^1D \leftarrow 1s^1S$ related feature is sharper in the short-lived spectrum than in the long-lived.

With increasing cluster size from N = 225 to N = 360, broad bands quickly evolve alongside the sharp peaks. We note, that these bands are apparently already evolved for cluster sizes where the VUV fluorescence spectrum hardly shows intensity, for example, between 23.1 eV and 23.6 eV. Because of the sensitivity of the normalised spectra to regions of low VUV fluorescence intensity, artefacts from the cluster size distribution can arise in regions where rapid changes with cluster size are observed. We nevertheless emphasise, that although the photo absorption may be low, it does not exclude quantum efficiency of NIR/VUV fluorescence being high.

The feature close to the atomic $2p^1P$ energy level, *Band B*, shows that transitions to lower lying electronically excited states are present in this region. Energy dispersive fluorescence spectroscopy shows that alongside the atomic $2p^1P \rightarrow 2s^1S$ transition a multitude of excimer transitions also take place, including from singlet states C, D, and higher having energies of 19.5 eV and 20.5 eV, respectively. These transitions show that the excited atoms are reactive and form excimers prior to ejection [‡] . However, the ef-

[‡] *It is very likely that the singlet states A (18.2 eV) and B (18.6 eV) are populated as*

ficiency of these transitions is rather low and always smaller than 10 %. In the energy range from 21.25 to 21.45 eV the short-lived correlated spectrum of N = 225 clusters shows higher intensity in *Band B* than the long-lived, likewise, the broad feature at 23.25 eV. This indicates that in this region non-radiative decay to lower lying states is comparatively efficient.

With the rise of bands, sharp dips at the np^1P transition energies are observed. The width of these dips is limited by the monochromator resolution.

Fig. 8 shows spectra of larger ^{4}He clusters. The normalised NIR/VIS fluorescence of excitations of *Band B* decreases in intensity with increasing cluster size. The broader feature at 23.25 eV evolves progressively into a double-structure. This trend can also be seen in the spectra of even larger ^4He_n clusters and droplets in Fig. 9. Overall, with increasing droplet size, the efficiency of NIR/VIS fluorescence decreases. The $3d^1D \leftarrow 1s^1S$ resonance disappears almost completely.

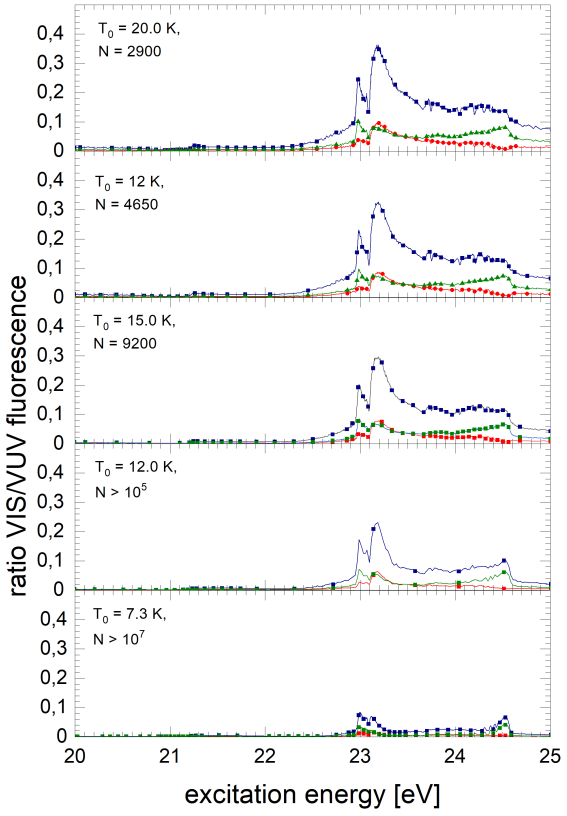

Fig. 9 Normalised NIR/VIS fluorescence spectra of very large ^4He_n clusters and droplets (blue filled squares). Short-lived normalised NIR/VIS fluorescence spectra are shown in red with filled circles and long-lived in green, with filled triangles.

well, however, transitions from b and B states were outside the spectrometer sensitivity range. To be published.

The spectrum of normalised very large ^{4}He droplets recorded at source temperatures lower than 15 K, and particularly that of T_0 = 7.3 K, are affected by artefacts related to limitations of VUV fluorescence measurements of large droplets mentioned above.

3.5 Normalised integral, short-lived and long-lived NIR/VIS spectra of ^3He_n

The normalised NIR/VIS fluorescence excitation spectra of ^{3}He droplets are shown in Fig. 10 and Fig. 11.

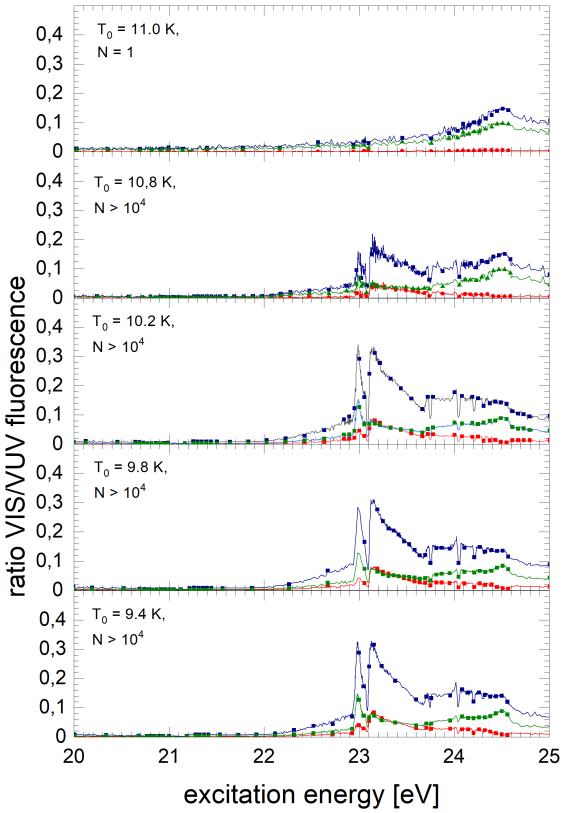

Fig. 10 Normalised NIR/VIS fluorescence excitation spectra for ^{3}He droplets for source temperatures in the range from 9.4 K to 11 K.

In broad terms, the normalised NIR/VIS fluorescence excitation spectra of ^{3}He droplets looks very similar to those of ^{4}He, however, the following differences should be noted: the intensity of the NIR/VIS fluorescence emerging from excitations of *Band B* is in all cases smaller than 8 %. The feature close to the $3s^1S \leftarrow 1s^1S$ dominates the spectrum with strong intensity, likewise, the feature peaking at 23.15 eV. The dips at the position of the np^1P energies are deeper than those of their ^{4}He counterparts, most likely indicating a higher percentage of uncondensed atoms in ^{3}He droplet beams than for ^{4}He.

With the exception of these dips, the NIR/VIS-VUV intensity ratio is always higher than for ^{4}He droplets of similar size at en-

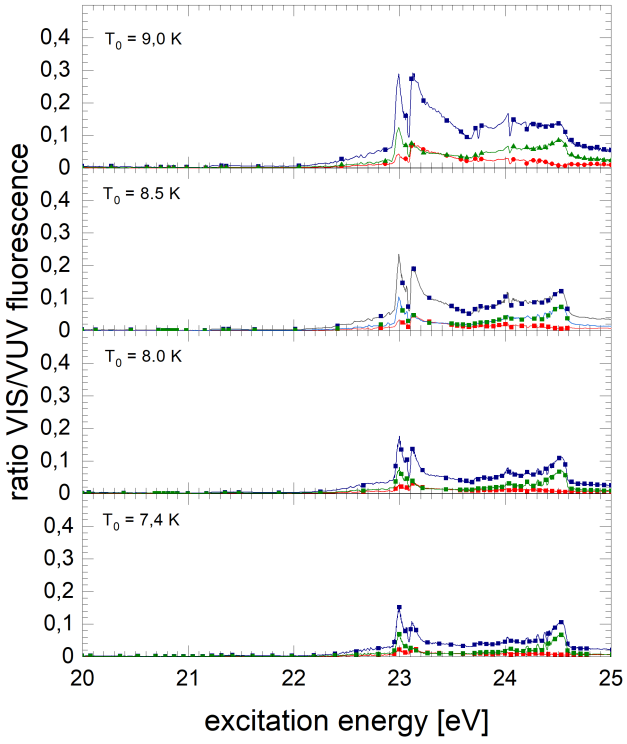

Fig. 11 Normalised NIR/VIS fluorescence excitation spectra for ^{3}He droplets for source temperatures in the range from 7.4 K to 9 K.

ergies of the $3s^1S \leftarrow 1s^1S$ resonance and above. This is particularly obvious for the long-lived fluorescence which is indicative for relaxation channels involving rapid ejection prior to competing non-radiative decay to lower lying states.

Like for ^{4}He droplets, the sharp peaks close to the atomic $3s^1S \leftarrow 1s^1S$, $4s^1S \leftarrow 1s^1S$, $5s^1S \leftarrow 1s^1S$ and $6s^1S \leftarrow 1s^1S$ transition energies are all blue-shifted with respect to the atomic transition energies, however, within the resolution of our apparatus, the magnitude of the shift is progressively smaller with increasing principal quantum number and also much better discernible than for ^{4}He. These shifts will be discussed in a forthcoming section.

Spectra of the NIR/VIS-VUV fluorescence ratio of large droplets of ^{3}He and ^{4}He are shown for comparison in Fig. 12 where these subtle features can be observed with greater clarity.

4 Discussion

4.1 General remarks

The electronically excited states of helium clusters and droplets are understood in terms of perturbed electronically excited atomic states for a number of reasons: being energetically very close, *Band A* and *Band B* are correlated with the atomic resonances $2s^1S \leftarrow 1s^1S$ and $2p^1P \leftarrow 1s^1S$, respectively[37,41]. Their orbital radii are smaller than the internuclear separation of bulk liquid helium. As a consequence, localised states can form[67,68]. For the higher states, the situation is more complex. The sharp peaks close to the atomic $ns^1S \leftarrow 1s^1S$ resonances have been attributed to perturbed atomic states of helium atoms that are lo-

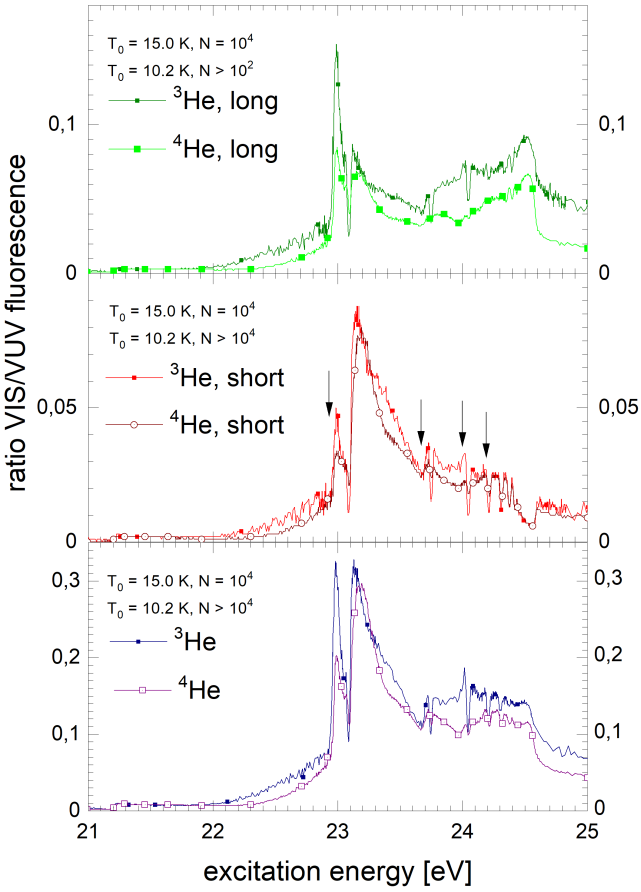

Fig. 12 Comparison of the normalised NIR/VIS fluorescence excitation spectra of large ^{3}He and ^{4}He droplets (N = 10^4). Long-lived, short-lived and integral normalised NIR/VIS fluorescence excitation spectra are shown from top to bottom. The features comprise sharp resonances (arrows indicating the atomic $ns^1S \leftarrow 1s^1S$ transition energies) and dips alongside broad bands. The features are shifted with respect to the atomic resonance energies. The NIR/VIS-VUV intensity ratio is higher for ^{3}He than for ^{4}He droplets, but not in the region of *Band B*. See text.

cated in the cluster surface region, which is characterised by a gradually decaying radial particle density over a region of 7 Å in thickness. A feature at higher energies, *Band E*, could be attributed to atomic-like states located at the surface and characterised by a principal quantum number n = 4 because its intensity depended on the cluster size in the specific way that is expected for surface states[39]. Features that would support an assignment of angular momentum have nevertheless not been identified yet. Therefore, we attribute this feature to '4l', with the letter 'l' indicating the unknown angular momentum.

It is established that after electronic excitation, helium clusters and droplets eject electronically excited helium atoms and excimers[47,73,76]. These emit fluorescence in the NIR/VIS spectral range due to transitions into lower lying electronically excited

states[73,76]. For very large droplets, excimers emit fluorescence also *within* bubbles *inside* the droplets[38]. There is evidence that the bubbles move within the droplets and, depending on isotopic composition, which affects the life- and residence time, reach the surface and release the excited atoms or molecules[38].

How these processes depend on the excitation energy, cluster size and localisation/delocalisation of the excitation as well as how they compete with other relaxation channels will be discussed in this section.

To facilitate the discussion, magnified normalised spectra of large ^{3}He and ^{4}He clusters (N = 10^4) are shown in Fig. 12.

4.2 Sharp intense peaks in the normalised NIR/VIS spectra

Table 1 Shifts of the maximum of the $3s^1S$-correlated features of ^4He_n with respect to the atomic $3s^1S$ level[88]. The third column shows the energy shifts in the NIR/VIS fluorescence excitation spectrum, the fourth column in the VUV spectrum and the fifths column shows the shifts in the normalised NIR/VIS spectrum. The spectra of the largest droplets, N = 10^5 and 10^7, are affected by artefacts as mentioned above and the reported shifts have to be treated with care.

N (atoms)	R (Å)	shift (eV) NIR/VIS - $3s^1S$	shift (eV) VUV - $3s^1S$	shift (eV) norm. - $3s^1S$
80	9.57	0.007	0.007	N.A.
225	13.50	0.007	0.046	0.007
280	14.52	0.015	0.049	0.015
360	15.79	0.048	0.073	0.036
450	17.01	0.048	0.075	0.044
570	18.41	0.044	0.070	0.048
720	19.90	0.048	0.070	0.05
1200	23.59	0.050	0.080	0.058
1800	27.00	0.058	0.080	0.058
2900	31.66	0.065	0.088	0.065
4650	37.05	0.070	0.093	0.068
9200	46.52	0.070	0.093	0.074
10^5	103.0	0.070	0.093	0.07
10^7	478.3	0.074	0.096	0.074

As mentioned above, the distinct sharp peaks previously observed in VUV fluorescence excitation spectra of helium clusters and droplets are attributed to transitions from the ground state to states localised at the surface of clusters and droplets. At the surface, the perturbation is low, favouring narrow spectral features and comparatively small spectral shifts. The energetic vicinity to the atomic dipole-forbidden $ns^1S \leftarrow 1s^1S$ resonances facilitates their assignment and indicates that these states have, to a large extent, s-character and nearly spherical symmetry[39]. It is indeed plausible that these states can form because at the surface there is sufficient free space to support n = 3 Rydberg orbitals. The formation of such large-orbital atomic-like states is further supported by the lower particle density within the surface region of helium clusters, decreasing smoothly from bulk values to zero, as mentioned above.

In the previous section, it is demonstrated that the NIR/VIS spectra largely follows the VUV spectra. Hence, sharp peaks are seen. The peaks are shifted with respect to the atomic $3s^1S$ energy. Their magnitude depends on the cluster size, however, compared to the VUV spectrum, the shifts are lower in magnitude. Also, in the *normalised* NIR/VIS spectra, the peaks are seen, however, again the peaks have slightly different shifts. The magnitude of these shifts is shown in Table 1 for all sizes of the ^{4}He clusters and droplets under investigation. Similarly, in Fig. 13, the cluster size dependence of the shifts of the $3s^1S \leftarrow 1s^1S$ transition with respect to the atomic transition is illustrated for the VUV, NIR/VIS and normalised NIR/VIS spectra.

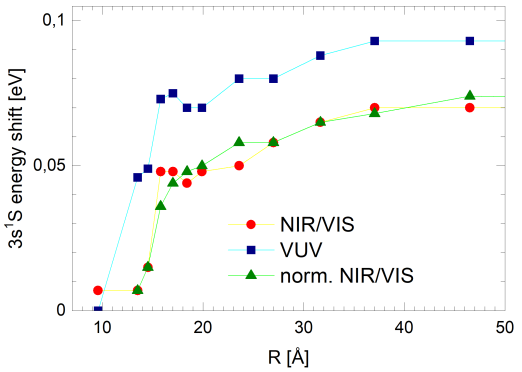

Fig. 13 Shifts of the peak energies of the $3s^1S \leftarrow 1s^1S$ transition with respect to the atomic transition observed in the VUV (blue squares), NIR/VIS (red spheres) and normalised NIR/VIS (green upper triangles) spectra. The lines are guides to the eye.

We will see below that it is reasonable to interpret the shifts seen in the normalised NIR/VIS spectra in terms of energy barriers. These barriers are obstacles along the reaction trajectory of electronically excited atoms in $3s^1S$ states, leading to their ejection from the cluster surface or to reactions with ground state helium atoms, forming He_2^* in excited states that are several eV lower than the atomic $3s^1S$ state. We can write the following photo reaction equations:

$$He_n + h\nu \quad \rightarrow \quad He_n^* \rightarrow He_{n-1} + He^* + \Delta E \qquad (1)$$

$$He_n + h\nu \quad \rightarrow \quad He_n^* \rightarrow He_{n-2} + He_2^* + \Delta E \qquad (2)$$

Equation 1 describes in simple terms the photo excitation of a helium cluster or droplet (on the left hand side) into a localised $3s^1S$ surface state (middle) followed by ejection of a helium atom in a $3s^1S$ excited state and generation of excess energy ΔE (on the right hand side). The magnitude of excess energy ΔE produced in this photo reaction is identical to the shift displayed in a fluorescence excitation spectrum and shown in table 1 for the whole range of ^{4}He cluster sizes under study. ΔE accounts for the generation of collective excitations (acoustic phonons, surface ripplons) in the helium clusters and droplets as well as the kinetic energy of the ejected helium atoms.

Equation 2 is very similar, however, here the excited surface atom reacts into an excimer. NIR/VIS fluorescence from singlet and triplet excimer states has been observed after excitation of the $3s^1S$ surface state[79]. The spectral lines of the fluorescence emitted from these excimers are unshifted with respect to the vacuum reference values, indicating that they emit after being ejected from the clusters. Also, their fluorescence is emitted from states, whose energies lie more than 3 eV below that of the $3s^1S$ surface

state. Prominent fluorescent bands emerge from these states, including the C, D, E states, having energies of 19.5 eV, 20.5 eV and 20.6 eV, respectively and their triplet counterparts[76]. Further details on the findings from energy dispersive spectroscopy will be published in a forthcoming article.

Thus, Fig. 13 illustrates how the barrier evolves with the cluster size. Small clusters appear to have very low barriers. Extrapolation suggests that for the smallest clusters a barrier hardly exists. With increasing cluster radius, R, the barrier height rises quickly. For clusters larger than $R = 18$ Å the barrier height increases only moderately, reaching a plateau of approximately 70 meV.

These findings are also non unexpected from the perspective of the small heat capacity of small helium clusters and their inability to support low-energy, i.e. long wavelength phonons[89,90]. As a consequence, small clusters cannot cope with the full excess energy in equations 1 and 2. Excitation of $3s^1S$ surface states of very small helium clusters are therefore most likely followed by subsequent ejection of atoms in $3s^1S$, without any further non-radiative relaxation involved.

This interpretation is supported by the time-correlated spectra. The $3s^1S \leftarrow 1s^1S$ resonance in the long-lived normalised fluorescence excitation spectra of small clusters shown in Fig. 7 has very high intensity – the highest in these spectra. The radiative lifetime of the $3s^1S$ state is 54.2 ns[84]. This matches the time-window of 40 to 172 ns ('long'). Therefore, the long-lived fluorescence is sensitive for fast ejection of excited 3s atoms and absence of non-radiative decay prior to the ejection.

Fig. 8 and 9 shows an asymmetry in the $3s^1S \leftarrow 1s^1S$ resonance in the long-lived normalised fluorescence excitation spectra of larger clusters. The resonance exhibits higher intensity on the low-energy side of the feature, which means that for excitation energies below the barrier, ejection of excited 3s atoms is the preferred relaxation channel.

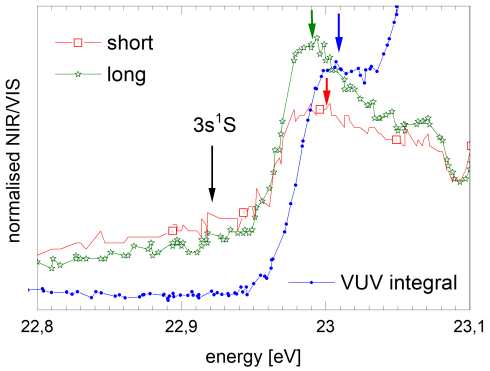

Fig. 14 Section view of Fig. 12 showing the region of the $3s^1S \leftarrow 1s^1S$ resonance in the short- and long-lived normalised fluorescence excitation spectra. The VUV-fluorescence excitation spectra is shown for comparison. Arrows indicate the energy of the atomic $3s^1S \leftarrow 1s^1S$ transition as well as the position of the maxima as displayed in table 1. The intensity scales are in arbitrary units, having been scaled to match the spectral features.

We will now discuss the short-lived normalised fluorescence spectrum – indicative for the non-radiative decay accompanying the fluorescence – providing further support for our interpretation. Fig. 14 shows a section view of Fig. 12, highlighting the observed asymmetry of the $3s^1S \leftarrow 1s^1S$ resonance in the long-lived normalised spectrum. The short-lived spectrum shows a plateaued $3s^1S \leftarrow 1s^1S$ resonance with a rather shallow maximum at slightly higher energies than the long-lived features. The centre of gravity is at even higher energies. We interpret this observation that with increasing excitation energy, it becomes more likely to overcome a barrier of height ΔE; more energy is flowing into non-radiative decay. We hypothesise that this excess energy is needed for the activation of the excited surface atom, reacting to become an excimer (equation 2), a process that occurs at the cost of the direct ejection of excited atoms (equation 1). The scenario is schematically illustrated in Fig.15.

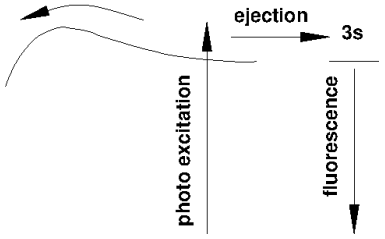

Fig. 15 Schematic showing the process of photo excitation of ns^1S correlated states (n = 3, 4, 5) and subsequent relaxation in the presence of an energy barrier. Excitations at energies below the barrier favours ejection of excited helium atoms in 3s, 4s, or 5s states. Energies above the barrier pave access to pathways that populate excimers states that are more than 3 eV lower in energy.

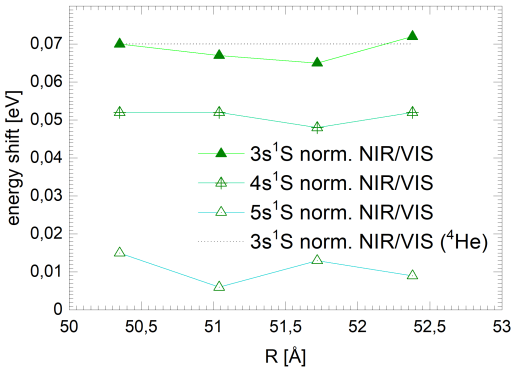

Fig. 16 Shifts of the $ns^1S \leftarrow 1s^1S$ resonance in the integral normalised fluorescence excitation spectra of medium-sized ^{3}He droplets, for principal quantum numbers $n = 3, 4, 5$. The dotted line shows the shift for ^{4}He droplets ($N = 10^4$)

For ^{3}He droplets, we are unable to produce similar data over a wide cluster size range because of their peculiar formation process in a beam, preventing us from producing small clusters in a controlled way. However, ^{3}He droplets serve as an interesting benchmark for higher ns^1S states because their resonance peaks are clearly discernible in the spectral data.

Fig. 12 shows, in addition to the 3s features, sharp resonances

close to the 4s and 5s states in the normalised NIR/VIS fluorescence excitation spectra of ^{3}He droplets. In the spectra of ^{4}He droplets, only 3s features can be identified with sufficient clarity. Like the 3s states, the 4s and 5s resonances are blue-shifted with respect to the atomic energy (see table 2). Fig.16 shows the magnitude of these shifts for each principal quantum number for several ^{3}He droplets of very similar sizes. The dotted line shows the corresponding magnitude of the 3s-shift for ^{4}He droplets (N = 10^4). It can be seen that the barrier heights decrease with principal quantum number. The fact that the barrier heights of the 3s resonances of ^{3}He and ^{4}He droplets have almost similar magnitudes indicates that electronic effects are very likely responsible, rather than density effects of the clusters or droplets. It is possible that these reactive processes take place in small electronically excited complexes within the surface of larger clusters and droplets, where these complexes can stabilise[91]. The absence of barriers in very small clusters could indicate that such centres require a minimum cluster size to fully stabilise. More experimental and theory work is needed to clarify theses questions. Blue-shifted features, correlated with the np singlet levels of He atoms, have been observed in the photo-absorption spectrum of dense He gas, indicating the presence of barriers[92]. In this work, a decrease of the blue-shift with principal quantum number, n, has been observed as well and related to the decrease of electron density.

Table 2 Energies and shifts of the maximum of the ns^1S-correlated features in the normalised NIR/VIS spectrum of ^{3}He$_n$ with respect to the atomic ns^1S levels[88]. The energies and shifts are averages of data from three very close sizes around N = 10^4 as shown in Fig. 16. The magnitudes of the shifts are interpreted as barrier heights.

n	energy (eV)	shift i.e. barrier height (meV)
3	22.9885	68.5
4	23.7250	51.0
5	24.0218	10.8

4.3 Broad 2p-related bands in the normalised NIR/VIS spectra

With increasing cluster size, the 2s- and 2p-related *Bands A* and *B* evolve to the dominating spectral features in VUV fluorescence excitation spectra[39], yet this is not seen in the NIR/VIS fluorescence excitation spectra (see Fig. 1 to Fig. 3). *Band A* is completely absent. Consequently, the *normalised* NIR/VIS fluorescence excitation spectra (see Fig. 7 to Fig. 9) show only weak intensity, progressively decreasing from less than 10 % for very small ^{4}He clusters to less than 1 % for the largest ^{4}He droplets.

This dramatic decrease is in stark contrast with the moderate decrease observed for the higher energy transitions. To shed light on this phenomenon, we have analysed the cluster size dependence of the normalised NIR/VIS fluorescence intensity in greater detail and established average intensities of the normalised NIR/VIS fluorescence for the 2p band in the region 21.21 eV - 21.75 eV, for 3s in the region 22.93 eV - 23.05 eV, for 3p in the region 23.15 eV - 23.5 eV and for 4l in the region 23.78 eV - 23.90 eV. The results are shown Fig. 17.

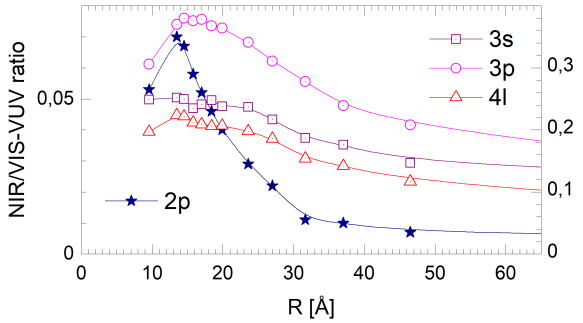

Fig. 17 Dependence of the NIR/VIS - VUV fluorescence intensity ratio on the radius, R, of ^{4}He clusters for selected spectral regions (see text). Note the different scales for 2p (left) and 3s, 3p and 4l (right). For 2p-related excitations, the normalised NIR/VIS fluorescence intensity decreases rapidly with cluster size. 3p is an intermediate case. For 3s and 4l the normalised NIR/VIS fluorescence intensity remains almost constant (see text). The range of R is limited to the region that is free from artefacts (see text).

With the exception of very small ^{4}He clusters (< 15Å), whose spectral features lie outside our integration range, see below, Fig. 17 shows that the normalised NIR/VIS fluorescence spectra decrease with cluster size. For the 2p band, this decrease is by more than a factor of 10. For the 3s and 4l band, the normalised NIR/VIS fluorescence spectra are almost constant. The 3p band is an intermediate case, showing a moderate decrease by a factor of two.

We recall that *Band A* and *B* have been attributed to perturbed 2s^{1}S and 2p^{1}P atomic-like states. This assignment is readily supported by the fact that the size of these orbitals fits within the space between the neighbouring ground state atoms. As this holds for any site, there is no preference for surface or bulk volume states.

Hence, we interpret the strong cluster-size-correlated decrease of the normalised NIR/VIS fluorescence intensity as the competition between VUV fluorescent decay (caused by direct transitions to the ground state) and resonant excitation transfer to a neighbouring atom. This type of transfer is terminated when (i) the excitation is localised in helium excimer states or when (ii) the surface is reached and an excited atom is ejected. Once excimers have formed, resonant transfer is no longer possible. The excimers can move freely in the helium clusters and transport energy towards the surface, albeit at much lower speed than via excitation hopping. At the surface, they are ejected and emit NIR/VIS fluorescence outside the clusters or droplets in vacuum. Unlike the 3s, 3p and higher states, including 4l, the 2p excited states are not restricted to the surface and are abundant throughout the cluster. Therefore, ejection and NIR/VIS fluorescence, the final step in the transfer of energy to the surface, become less and less likely when the cluster size increases.

In larger droplets, one expects an increased likelihood for the excitation energy to localise in excimers states because of the longer excitation hopping trajectory. In fact, an increase of fluorescence from excimers with increasing clusters size has already been observed in experiment[76,79] and will be investigated in more detail in the future. Fluorescent NIR/VIS transitions includ-

ing from high vibrational states up to v = 5 have been observed, notably C $^1\Sigma_g^+ \rightarrow$A $^1\Sigma_u^+$ and D $^1\Sigma_u^+ \rightarrow$B $^1\Pi_g$. An investigation of the spectral region around the D $^1\Sigma_u^+ \rightarrow$B $^1\Pi_g$ transition showed that inside large helium droplets excimers emit fluorescence within bubbles alongside fluorescence from ejected species in vacuum[38]. It is expected that bubbles will stabilise around other spherically symmetric excited states, including the C $^1\Sigma_g^+$, its triplet counterpart and the atomic 3s^{1}S and 3s^{3}S states, but not in connection with non-spherical states such as the E $^1\Pi_g$ which have been identified in the fluorescence spectrum[38]. Recently, bubble formation around the 2s^{1}S state has been studied[49].

Therefore, the strong decrease of the intensity of the normalised NIR/VIS fluorescence intensity with cluster size is readily explained by energy transfer processes competing with direct fluorescent decay to the ground state. After population of an excited perturbed atom within the cluster, excitation transfer by resonant hopping takes place. Previous work and our data suggest that the excitation moves first in a random walk fashion until the energy localises in an excimer state, forming a bubble. The bubble would then travel ballistically towards the surface, owing to the superfluid state of the ^{4}He droplets[38]. The negative linear slope of the normalised NIR/VIS fluorescence intensity supports this interpretation.

We note that, as mentioned before, for very large ^{4}He droplets the normalised NIR/VIS fluorescence intensity is affected by artefacts. Therefore only the range of radii is shown where the spectral features are free of these artefacts.

4.4 Broad 3s, 3p and 4l-related bands in the normalised NIR/VIS spectra

The fact that the normalised NIR/VIS fluorescence intensity for the 3s and 4l-related states remains almost constant is readily explained by their localisation at the surface. It is reasonable to assume that fast ejection of excited atoms must be an efficient relaxation channel when the originating state is close to the surface. In the previous section, we have seen that ejection of excited atoms competes with non-radiative relaxation into electronically excited states of lower energy, including He excimer states more than 3 eV below than the 3s^1S state.

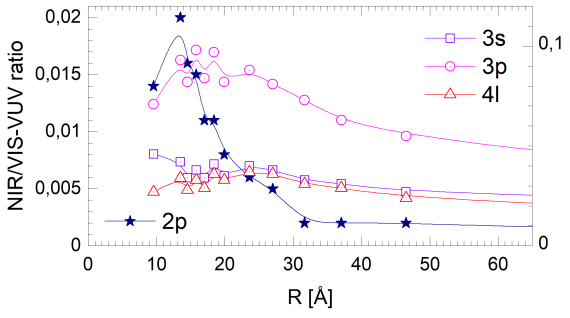

Fig. 18 Short-lived normalised NIR/VIS fluorescence intensity dependence on the radius, R, of ^{4}He clusters for selected spectral regions (see text and Fig. 17). Note the different scales.

To assess the cluster and droplet size dependence of non-radiative relaxation, the normalised short-lived NIR/VIS fluorescence is illustrated in Fig. 18. The lines connecting the 3s, 3p and 4l data points are very similar to their counterparts in Fig. 17. The decrease with droplet size is even smaller, showing hardly any dependence on the droplet size. This supports the interpretation that non-radiative relaxation is very efficient at the cluster and droplet surface.

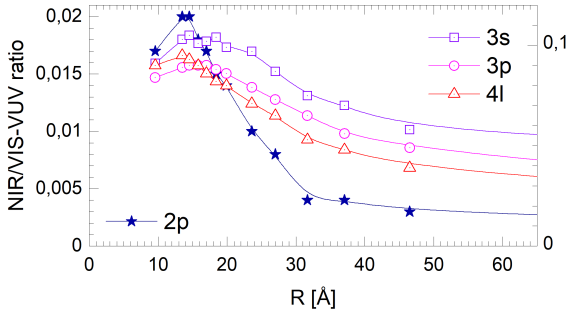

Fig. 19 Dependence of the long-lived normalised NIR/VIS fluorescence intensity on the radius, R, of ^{4}He clusters for selected spectral regions (see text and Fig. 17). Note the different scales.

The corresponding data for the long-lived NIR/VIS fluorescence is shown in Fig. 19. All lines connecting the 3s, 3p and 4l data points show a moderate decrease with droplet size. This finding can be interpreted in terms of (i) a wider surface area being involved in the fast ejection of atoms or (ii) by the lower particle density in the surface region, effectively promoting fast ejection.

Firstly, the width of the surface area targeted during photo excitation defines the duration of the journey of the excitation towards the surface and the increasing likelihood of direct decay to the ground state, producing VUV fluorescence. It is plausible that the width of this area is defined by the size of the involved orbitals and the region where the particle density decreases from the bulk value to zero (7 - 10Å). The data suggests that fast ejection appears to be triggered by photo excitation of states in this entire surface layer.

Secondly, the lower particle density in the surface area readily explains an increase of efficiency of fast ejection because the likelihood of collisions with ground state atoms decreases. For increasing average cluster and droplet sizes, the contribution of surface effects to the ensemble decreases, hence, a moderate decrease in the overall ejection rate comes not unexpected and is in fact observed in Fig. 19.

4.5 Absence of 2s-related bands in the NIR/VIS spectra

The absence of the 2s-related features in the NIR/VIS fluorescence excitation spectra indicates that a considerable part of the excitation energy is transferred into the $A^1\Sigma_u^+$ excimer state or into 2s^1S He atoms, which subsequently desorb[49]. Most of the VUV fluorescence is due to the dipole-allowed $A^1\Sigma_u^+ \rightarrow X^1\Sigma_g^+$ transition[73,93] of He excimer molecules, whereas radiative decay of 2s^1S He atoms is dipole-forbidden.

4.6 Comparison between ^{3}He and ^{4}He clusters and droplets

Fig. 20, 21 and 22 show the normalised NIR/VIS fluorescence intensity in selected energy bands for (N = 10^4) large ^{3}He and ^{4}He droplets, for comparison. Owing to the much lower NIR/VIS fluorescence efficiency of the 2p features, different scales are used, with the left hand side scales for the 2p features, and the right for 3s, 3p and 4l.

The NIR/VIS fluorescence quantum yields of large droplets shown in Fig. 20, 21 and 22 are consistent with the finding discussed above. Large ^{3}He droplets exhibit a very low NIR/VIS fluorescence quantum yield for the 2p correlated excitation that differs from that of ^{4}He droplets by less than 50%. For the investigated 3s, 3p and 4l bands, the normalised NIR/VIS fluorescence is higher and very similar to the values of ^{4}He droplets of similar size for the integral and short-lived fluorescence.

A notable difference is observed in Fig. 22 for the long lived fluorescence. Whereas 3p and 4l data points are almost on top of each other, and also rather close to the ^{4}He data points, the 3s normalised NIR/VIS fluorescence, showing a quantum yield of 0.09, is 1.5 times stronger than for ^{4}He droplets, which show a quantum yield of 0.06. Building on our findings and discussion above, particularly in relation to Fig. 19, this result is readily explained by lower particle density facilitating rapid ejection of excited atoms from photo-excited states in the surface region. The increase of normalised NIR/VIS fluorescence by 150% is broadly related with the density ratio of 1.33 between bulk liquid ^{4}He and bulk liquid ^{3}He.

In relation to the discussion of cluster size dependence of ^{4}He illustrated in Fig. 19, we emphasise the aspect that ^{3}He droplet beams are free of contributions from small clusters. By comparison, it is often possible to distinguish features related to the low particle density as displayed in the surface region of helium clusters or in ^{3}He droplet from size-related effects such as confinement. In this respect, the ^{3}He data shown in Fig. 22 may provide valuable benchmark information.

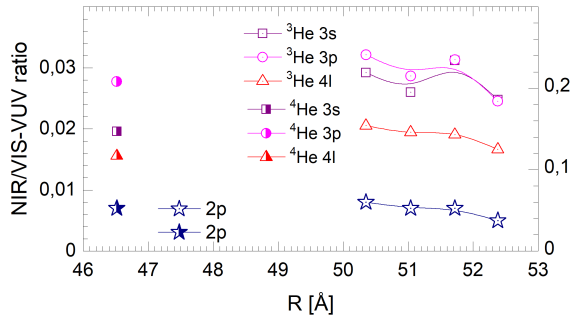

Fig. 20 Droplet radius dependence of the normalised integral NIR/VIS fluorescence. The scale on the right applies for the 3s, 3p and 4l labelled features of both ^{3}He and ^{4}He droplets. The scale on the left applies for 2p for both ^{3}He and ^{4}He droplets. Some of the data points shown refer directly to the spectra in Fig. 12.

4.7 Relaxation

Taking the observed isotope, cluster-size, energy and time-correlation dependence of the NIR/VIS fluorescence into account,

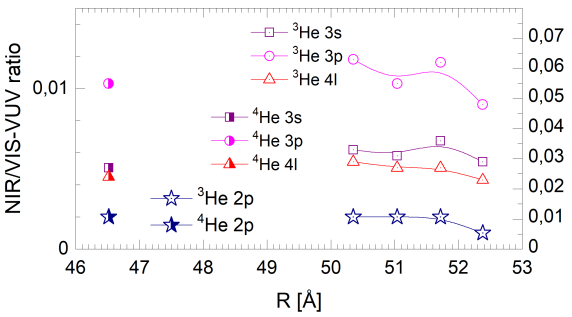

Fig. 21 Droplet radius dependence of the normalised short-lived NIR/VIS fluorescence. Scales like in Fig. 20.

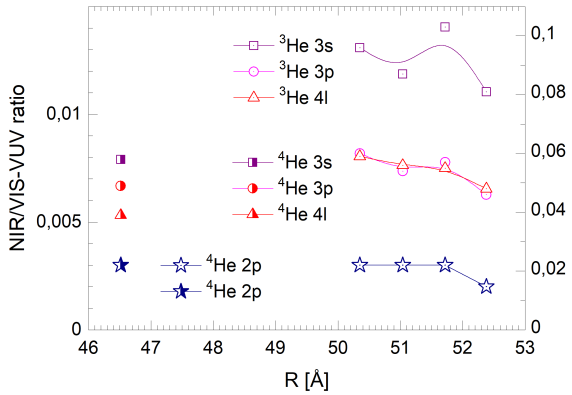

Fig. 22 Droplet radius dependence of the normalised long-lived NIR/VIS fluorescence. Scales like in Fig. 20.

the relaxation dynamics of electronically excited helium clusters and droplets can be understood in terms of perturbed atomic states, particle density and orbital size/principal quantum number.

Fig. 23 shows schematically how these factors influence the efficiency of ejection of excited helium atoms with emphasis on the role of excitation energy. A VUV fluorescence excitation spectrum of ^{4}He droplets, which is to a good approximation proportional to the absorption spectrum, is shown as guidance.

At high energies, in the region between 23 eV and the vertical ionisation threshold, the excitations of helium clusters and droplets are localised at the surface. While after population of these states, VUV fluorescence is the most important relaxation channel, relaxation can also proceed via (i) fast ejection of excited atoms from the surface, which subsequently emit NIR/VIS fluorescence or (ii) non-radiative relaxation into lower lying states, which may then result in the ejection of atoms or excimers and subsequent NIR/VIS fluorescence. At energies close to the ns^{1}S resonances, indicated by areas in orange colour in Fig. 23, process (i) is facilitated by the low particles density within the outer surface region and can account for an efficiency of up to 70 %. The absorption bands in between, indicated by yellow-green colour, support process (ii). Non-radiative relaxation at the surface is characterised by the presence of energy barriers whose heights depend on the principal quantum number n.

At low energies, in the region around the 2p energy, relaxation

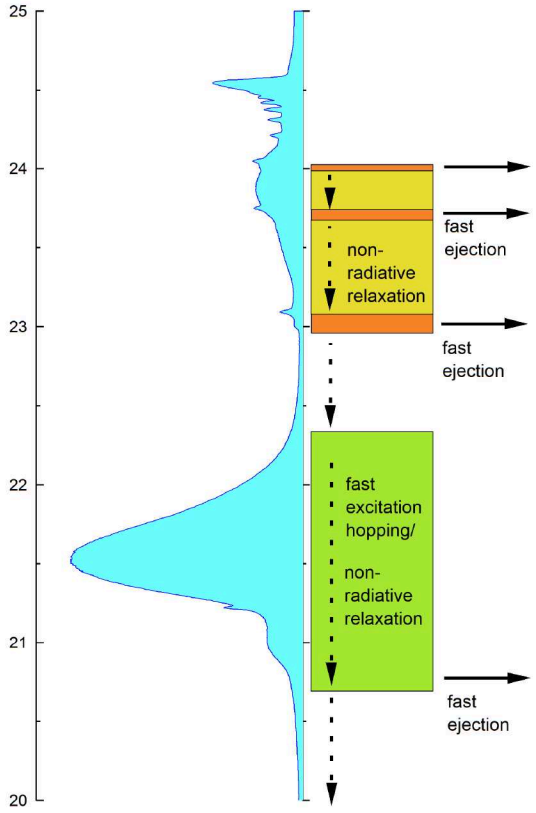

Fig. 23 Schematic illustrating the dominating relaxation channels. The vertical scale gives the excitation energy in eV. A VUV fluorescence excitation spectrum of ^{4}He droplets (N = 10) is shown, which to a good approximation represents the photo absorption spectrum. On the right hand side, prevailing non-radiative energy transfer and decay mechanism are indicated, including fast ejection. Horizontal arrows indicate energy regions where atoms and excimers are ejected even more rapidly. These processes depend on the principal quantum number, n, and the location of the excitations. The dashed vertical arrows indicate non-radiative decay to electronically excited states that are lower in energy, including singlet and triplet excimer states in the region between 19.2 and 21.4 eV.

is characterised by resonant excitation transfer. Transfer of energy to the surface competes strongly with direct fluorescent decay to the ground state. It becomes less and less likely with increasing cluster size which is reflected by much lower NIR/VIS fluorescence efficiency, decreasing from 10% to less than 1%.

Fig. 24 illustrates these processes in a simplified cross-sectional view, highlighting the role of cluster size and orbital-size. For simplicity, the random-walk of excitation hopping is not shown. After random-walk-hopping, the excitation localises within bubbles which, in the case of normal liquid ^{3}He, then move towards the surface in a random walk fashion or, in the case of superfluid ^{4}He, via ballistic trajectories[38].

The fluorescence spectroscopy results presented here complement recent photoemission results[49,78]. While important trends, such as rapid relaxation, are similar, some details, in particular the branching ratios of the different relaxation channels, appear to be different and need to be clarified in future work [‡].

[‡]*Personal communication with M. Mudrich.*

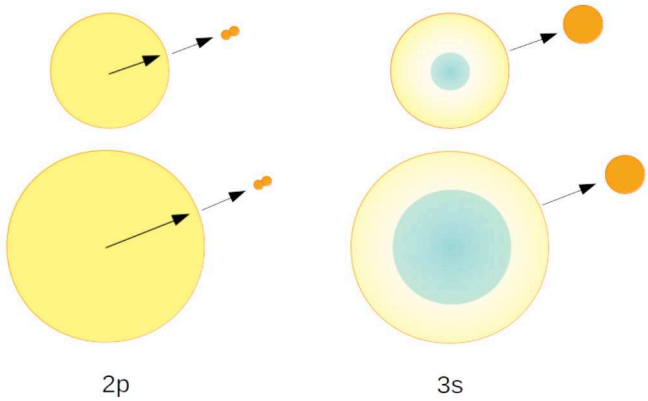

Fig. 24 Schematic illustrating the prevailing relaxation channels for 2p and 3s related levels. The top and bottom rows represents small and large clusters, respectively. The 2p-related excitations are de-localised, whereas 3s and higher excitations are restricted to the surface region. As a consequence, the efficiency of ejection of highly excited atoms and excimers from the surfaces decreases for 2p related states with increasing cluster size, whereas for higher excitations this efficiency remains constant. For simplicity, random-walk and localisation features are not illustrated.

5 Conclusion

In summary, the relaxation of electronically excited ^{3}He and ^{4}He clusters and droplets has been investigated. Time-correlated fluorescence excitation spectroscopy with selective detection in the NIR/VIS range, spanning a wide range of cluster and droplet sizes has been employed. Previous work had shown that the NIR/VIS fluorescence is indicative for the ejection of excited atoms and excimers. However, for a comprehensive understanding of the relaxation dynamics, detailed spectroscopic data was required.

With regard to their shape, the NIR/VIS fluorescence excitation spectra were found to be broadly similar to the VUV fluorescence excitation spectra. However, when the fluorescence excitation spectra were normalised to the VUV fluorescence, distinct differences were observed. The most striking difference between the NIR/VIS and the VUV fluorescence excitation spectra is the much lower intensity in the 2p region compared to excitations at n = 3 and higher principal quantum numbers. Also, the 2s-related *band A* is absent.

The distinct cluster size dependence observed in the normalised NIR/VIS fluorescence excitation spectra confirmed the tentative assignment of atomic-like surface states with principal numbers of n = 3 and higher from previous work. Furthermore, evidence was found that that the dynamics of the relaxation differed between states of n = 2 and n $\geq$ 3 principal quantum numbers.

Owing to the relatively large internuclear separation in liquid helium, the size of the wavefunctions related to the n = 2 states fits well within the space between neighbouring atoms. As a consequence, atomic-like states can exist with only moderate perturbation of the 2s and 2p levels. This is no-longer the case for n = 3 where the size of the orbitals greatly exceeds internuclear separation. The surface of helium clusters or droplets is an exception. At the surface, there is free space in the direction of the surface normal vector. Furthermore, the region is characterised by a particle

density that smoothly decreases from bulk densities to zero. Depending on the location within this surface layer, the existence of s-states related to n = 4 principal quantum numbers and higher could be established.

The efficiency of the fast ejection of atoms and excimers is very high for photo excitation of these surface states, leading to a high NIR/VIS yield regardless of the cluster and droplet size. For the 2p-related case, the NIR/VIS yield is low and decreases with cluster size because the energy has to hop across the clusters or droplets which competes with non-radiative decay to lower states and VUV fluorescence to the ground state.

Non-radiative decay competing with fast, direct ejection of helium atoms was also identified at the surface. A barrier separates these two processes. The barrier height was found to decrease with increasing quantum number *n*.

Our interpretation is strongly supported by the findings for ^{3}He droplets, which serve as a test ground for the variation of particle density. The distinctly lower particle density in ^{3}He droplets makes fast ejection of excited surface atoms more efficient.

Author Contributions

All authors have contributed to setting-up the experiment and acquiring the data. In addition, KvH and TM have contributed to the interpretation of the data. KvH has written the manuscript, with contributions from other authors.

Conflicts of interest

There are no conflicts to declare.

Acknowledgements

KvH acknowledges support through COST action CA211012022-10-03 and in-kind contributions by Kanano GmbH. We are grateful to Isabella von Haeften for proof-reading the manuscript.

Dedication

This contribution is dedicated to the themed collection 'Electronic and Nuclear Dynamics and their Interplay in Molecules, Clusters, and on Surfaces: Festschrift for Wolfgang E. Ernst' in honour of Professor Wolfgang Ernst's 70th birthday.

Notes and references

1 J. Gspann and G. Krieg, *J. Chem. Phys.*, 1974, **61**, 4037.
2 E. Becker, *Z. Phys. D At. Mol. Clus.*, 1986, **3**, 101–107.
3 J. P. Toennies and A. F. Vilesov, *Ann. Rev. Phys. Chem.*, 1998, **49**, 1–41.
4 J. A. Northby, *J. Chem. Phys.*, 2001, **115**, 10065–10077.
5 F. Stienkemeier and A. F. Vilesov, *J. Chem. Phys.*, 2001, **115**, 10119.
6 K. von Haeften and M. Havenith, *Electronic Excitations in Liquefied Rare Gases*, American Scientific Publishers, Los Angeles, CA, USA, 2005.
7 J. Küpper and J. Merritt, *Int. Rev. Phys. Chem.*, 2007, **26**, 249–287.
8 T. Fennel, K.-H. Meiwes-Broer, J. Tiggesbäumker, P.-G. Reinhard, P. M. Dinh and E. Suraud, *Rev. Mod. Phys*, 2010, **82**, 1793.
9 S. Yang and A. M. Ellis, *Chem. Society Rev.s*, 2013, **42**, 472–484.
10 M. Mudrich and F. Stienkemeier, *Int. Rev. Phys. Chem.*, 2014, **33**, 301–339.
11 M. P. Ziemkiewicz, D. M. Neumark and O. Gessner, *Int. Rev. Phys. Chem.*, 2015, **34**, 239–267.
12 A. Mauracher, O. Echt, A. Ellis, S. Yang, D. Bohme, J. Postler, A. Kaiser, S. Denifl and P. Scheier, *Phys. Rep.*, 2018, **751**, 1–90.
13 C. Bostedt, T. Gorkhover, D. Rupp and T. Möller, *Synchrotron light sources and free-electron lasers: Accelerator physics, instrumentation and science applications*, 2020, 1525–1573.
14 W. Schöllkopf and J. P. Toennies, *Science*, 1994, **266**, 1345–1348.
15 G. Galinis, C. Cacho, R. T. Chapman, A. M. Ellis, M. Lewerenz, L. G. M. Luna, R. S. Minns, M. Mladenović, A. Rouzée, E. Springate, I. C. E. Turcu, M. J. Watkins and K. von Haeften, *Phys. Rev. Lett.*, 2014, **113**, 043004.
16 T. E. Gough, M. Mengel, P. A. Rowntree and G. Scoles, *J. Chem. Phys.*, 1985, **83**, 4958–4961.
17 M. Lewerenz, B. Schilling and J. P. Toennies, *J. Chem. Phys.*, 1995, **102**, 8191–8207.
18 J. Higgins, C. Callegari, J. Reho, F. Stienkemeier, W. Ernst, K. Lehmann, M. Gutowski and G. Scoles, *Science*, 1996, **273**, 629.
19 J. Nagl, G. Auböck, C. Callegari and W. Ernst, *Phys. Rev. Lett.*, 2007, **98**, 75301.
20 F. Stienkemeier, J. Higgins, W. E. Ernst and G. Scoles, *Phys. Rev. Lett.*, 1995, **74**, 3592–3595.
21 A. Bartelt, J. D. Close, F. Federmann, N. Quaas and J. P. Toennies, *Phys. Rev. Lett.*, 1996, **77**, 3525–3528.
22 T. Diederich, T. Döppner, J. Braune, J. Tiggesbäumker and K.-H. Meiwes-Broer, *Phys. Rev. Lett.*, 2001, **86**, 4807–4810.
23 S. Yang, A. M. Ellis, D. Spence, C. Feng, A. Boatwright, E. Latimer and C. Binns, *Nanoscale*, 2013, **5**, 11545–11553.
24 G. Haberfehlner, P. Thaler, D. Knez, A. Volk, F. Hofer, W. E. Ernst and G. Kothleitner, *Nat. Commun.*, 2015, **6**, 1–6.
25 F. Lackner, in *Molecules in Superfluid Helium Nanodroplets*, Springer, 2022, pp. 513–560.
26 F. Laimer, L. Kranabetter, L. Tiefenthaler, S. Albertini, F. Zappa, A. M. Ellis, M. Gatchell and P. Scheier, *Phys. Rev. Lett.*, 2019, **123**, 165301.
27 L. Tiefenthaler, J. Ameixa, P. Martini, S. Albertini, L. Ballauf, M. Zankl, M. Goulart, F. Laimer, K. von Haeften, F. Zappa *et al.*, *Rev. Sci. Instrum.*, 2020, **91**, 033315.
28 M. Hartmann, R. E. Miller, J. P. Toennies and A. F. Vilesov, *Phys. Rev. Lett.*, 1995, **75**, 1566.
29 K. Nauta and R. E. Miller, *Phys. Rev. Lett.*, 1999, **82**, 4480–4483.
30 K. Nauta and R. E. Miller, *Science*, 1999, **283**, 1895–1897.
31 K. von Haeften, A. Metzelthin, S. Rudolph, V. Staemmler and M. Havenith, *Phys. Rev. Lett.*, 2005, **95**, 215301.
32 J. Tang, Y. Xu, A. R. W. McKellar and W. Jäger, *Science*, 2002,

297, 2030–2033.
33 A. S. Chatterley, C. Schouder, L. Christiansen, B. Shepperson, M. H. Rasmussen and H. Stapelfeldt, *Nat. Commun.*, 2019, **10**, 133.
34 A. S. Chatterley, L. Christiansen, C. A. Schouder, A. V. Jørgensen, B. Shepperson, I. N. Cherepanov, G. Bighin, R. E. Zillich, M. Lemeshko and H. Stapelfeldt, *Phys. Rev. Lett.*, 2020, **125**, 013001.
35 S. Grebenev, J. Toennies and A. Vilesov, *Science*, 1998, **279**, 2083.
36 M. Fárník, U. Henne, B. Samelin and J. P. Toennies, *Phys. Rev. Lett.*, 1998, **81**, 3892.
37 K. von Haeften, T. Laarmann, H. Wabnitz and T. Möller, *Phys. Rev. Lett.*, 2001, **87**, 153403.
38 K. von Haeften, T. Laarmann, H. Wabnitz and T. Möller, *Phys. Rev. Lett.*, 2002, **88**, 233401.
39 K. von Haeften, T. Laarmann, H. Wabnitz, T. Möller and K. Fink, *J. Phys. Chem. A*, 2011, **25**, 7316–7326.
40 D. Verma, S. M. O'Connell, A. J. Feinberg, S. Erukala, R. M. P. Tanyag, C. Bernando, W. Pang, C. A. Saladrigas, B. W. Toulson, M. Borgwardt *et al.*, *Phys. Rev. B*, 2020, **102**, 014504.
41 M. Joppien, R. Karnbach and T. Möller, *Phys. Rev. Lett.*, 1993, **71**, 2654–2657.
42 S. Yurgenson, C.-C. Hu, C. Kim and J. A. Northby, *Eur. Phys. J. D - At., Mol., Opt., Plasma Phys.*, 1999, **9**, 153–157.
43 D. S. Peterka, A. Lindinger, L. Poisson, M. Ahmed and D. M. Neumark, *Phys. Rev. Lett.*, 2003, **91**, 043401.
44 O. Kornilov, C. Wang, O. Bünermann, A. T. Healy, M. Leonard, C. Peng, S. Leone, D. Neumark and O. Gessner, *J. Phys. Chem. A*, 2010, **114**, 1437–1445.
45 O. Bünermann, O. Kornilov, S. R. Leone, D. M. Neumark and O. Gessner, *IEEE J. of Selected Topics in Quantum Electronics*, 2011, **18**, 308–317.
46 O. Kornilov, O. Bünermann, D. Haxton, S. Leone, D. Neumark and O. Gessner, *J. Phys. Chem. A*, 2011, **115**, 7891.
47 O. Bünermann, O. Kornilov, D. J. Haxton, S. R. Leone, D. M. Neumark and O. Gessner, *J. Chem. Phys.*, 2012, **137**, 214302.
48 M. P. Ziemkiewicz, C. Bacellar, K. R. Siefermann, S. R. Leone, D. M. Neumark and O. Gessner, *J. Chem. Phys.*, 2014, **141**, 174306.
49 M. Mudrich, A. LaForge, A. Ciavardini, P. O'Keeffe, C. Callegari, M. Coreno, A. Demidovich, M. Devetta, M. D. Fraia, M. Drabbels *et al.*, *Nat. Commun.*, 2020, **11**, 1–7.
50 C. M. Surko and F. Reif, *Phys. Rev.*, 1968, **175**, 229.
51 C. M. Surko and F. Reif, *Phys. Rev. Lett.*, 1968, **20**, 582.
52 C. M. Surko, G. J. Dick, F. Reif and W. C. Walker, *Phys. Rev. Lett.*, 1969, **23**, 842.
53 W. S. Dennis, J. E. Durbin, W. A. Fitzsimmons, O. Heybey and G. K. Walters, *Phys. Rev. Lett.*, 1969, **23**, 1083–1086.
54 J. W. Keto, M. Stockton and W. A. Fitzsimmons, *Phys. Rev. Lett.*, 1972, **28**, 792–795.
55 J. W. Keto, F. J. Soley, M. Stockton and W. A. Fitzsimmons, *Phys. Rev. A*, 1974, **10**, 872–886.
56 J. W. Keto, F. J. Soley, M. Stockton and W. A. Fitzsimmons, *Phys. Rev. A*, 1974, **10**, 887.
57 Z. Li, N. Bonifaci, A. Denat and V. Atrazhev, *IEEE transactions on dielectrics and electrical insulation*, 2006, **13**, 624–631.
58 Z.-L. Li, N. Bonifaci, F. Aitken, A. Denat, K. von Haeften, V. Atrazhev and V. Shakhatov, *Eur. Phys. J. - Appl. Phys.*, 2009, **47**, 22821.
59 N. Bonifaci, F. Aitken, V. M. Atrazhev, S. L. Fiedler and J. Eloranta, *Phys. Rev. A*, 2012, **85**, 042706.
60 V. V. Khmelenko, S. Mao, A. Meraki, S. C. Wilde, P. McColgan, A. A. Pelmenev, R. E. Boltnev and D. M. Lee, *Phys. Rev. Lett.*, 2013, **111**, 183002.
61 L. G. Mendoza-Luna, M. Watkins, K. von Haeften, N. Bonifaci and F. Aitken, *Eur. Phys. J. D*, 2013, **67**, 1–6.
62 L. G. Mendoza-Luna, N. M. K. Shiltagh, M. J. Watkins, N. Bonifaci, F. Aitken and K. von Haeften, *J. Phys. Chem. Lett.*, 2016, **7**, 4666 – 4670.
63 R. Carman, R. Ganesan and D. Kane, *J. Phys. D: Appl. Phys.*, 2016, **49**, 085201.
64 N. M. K. Shiltagh, L. G. Mendoza-Luna, M. J. Watkins, S. Thornton and K. von Haeften, *Eur. Phys. J. D*, 2018, **72**, 5.
65 A. Hickman and N. Lane, *Phys. Rev. Lett.*, 1971, **26**, 1216–1219.
66 F. J. Soley and W. A. Fitzsimmons, *Phys. Rev. Lett.*, 1974, **32**, 988–991.
67 K. von Haeften and K. Fink, *Eur. Phys. J. D: At. Mol. Opt. Plas. Phys*, 2007, **43**, 121–124.
68 K. D. Closser and M. Head-Gordon, *J. Phys. Chem. A*, 2010, **114**, 8023–8032.
69 K. D. Closser, O. Gessner and M. Head-Gordon, *J. Chem. Phys.*, 2014, **140**, 134306.
70 K. D. Closser, Q. Ge, Y. Mao, Y. Shao and M. Head-Gordon, *J. Chem. Theory Comput.*, 2015, **11**, 5791–5803.
71 S. L. Fiedler and J. Eloranta, *J. Low. Temp. Phys.*, 2014, **174**, 269–283.
72 H. Farrokhpour and M. Dehdashti-Jahromi, *J. Mol. Liq.*, 2017, **230**, 190–199.
73 K. von Haeften, T. Laarmann, H. Wabnitz and T. Möller, *J. Phys. B, At. Mol. Opt. Phys.*, 2005, **38**, S373–S386.
74 F. Ancilotto, M. Pi, R. Mayol, M. Barranco and K. Lehmann, *J. Phys. Chem. A*, 2007, **111**, 12695–12701.
75 E. Loginov and M. Drabbels, *Phys. Rev. Lett.*, 2011, **106**, 083401.
76 K. von Haeften, A. R. B. de Castro, M. Joppien, L. Moussavizadeh, R. von Pietrowski and T. Möller, *Phys. Rev. Lett.*, 1997, **78**, 4371–4374.
77 Y. Ovcharenko, A. LaForge, B. Langbehn, O. Plekan, R. Cucini, P. Finetti, P. O'Keeffe, D. Iablonskyi, T. Nishiyama, K. Ueda *et al.*, *New J. Phys.*, 2020, **22**, 083043.
78 J. D. Asmussen, R. Michiels, K. Dulitz, A. Ngai, U. Bangert, M. Barranco, M. Binz, L. Bruder, M. Danailov, M. Di Fraia, J. Eloranta, R. Feifel, L. Giannessi, M. Pi, O. Plekan, K. C. Prince, R. J. Squibb, D. Uhl, A. Wituschek, M. Zangrando,

C. Callegari, F. Stienkemeier and M. Mudrich, *Phys. Chem. Chem. Phys.*, 2021, **23**, 15138–15149.
79 K. von Haeften, *Ph.D. thesis*, University of Hamburg, DESY, 1999.
80 J. Harms, J. P. Toennies and F. Dalfovo, *Phys. Rev. B*, 1998, **58**, 3341.
81 R. Karnbach, M. Joppien, J. Stapelfeldt, J. Wörmer and T. Möller, *Rev. Sci. Instrum.*, 1993, **64**, 2838–2849.
82 N. Schwentner, E. Koch and J. Jortner, *Electronic excitations in condensed rare gases*, Springer, New York, Berlin, 1985.
83 T. Möller, A. De Castro, K. von Haeften, A. Kolmakov, T. Laarmann, O. Löfken, C. Nowak, F. Picucci, M. Riedler, C. Rienecker *et al.*, *J. El. Spectr. Rel. Phen.*, 1999, **101**, 185–191.
84 A. A. Radzig and B. M. Smirnov, *Reference Data on Atoms, Molecules and Ions*, Springer-Verlag, Berlin, Heidelberg, New York, Tokyo, 1985.
85 A. P. M. Barranco, J. Navarro, *Phys. Rev. Lett.*, 1997, **78**, 4729.
86 J. Harms, J. Toennies, M. Barranco and M. Pi, *Phys. Rev. B*, 2001, **63**, 184513.
87 A. Kramida, Yu. Ralchenko, J. Reader and and NIST ASD Team, NIST Atomic Spectra Database (ver. 5.10), [Online]. Available: `https://physics.nist.gov/asd` [2022, November 17]. National Institute of Standards and Technology, Gaithersburg, MD., 2022.
88 W. C. Martin, *J Res Natl Inst Stand. Section A, Phys. and Chem.*, 1960, **64**, 19.
89 K. von Haeften, S. Rudolph, I. Simanovski, M. Havenith, R. E. Zillich and K. B. Whaley, *Phys. Rev. B*, 2006, **73**, 054502.
90 R. E. Zillich, K. B. Whaley and K. von Haeften, *J. Chem. Phys.*, 2008, **128**, 094303.
91 T. Laarmann, A. Kanaev, K. von Haeften, H. Wabnitz, R. von Pietrowski and T. Möller, *J. Chem. Phys.*, 2002, **116**, 7558–7563.
92 V. Guzielski, M. Castex, J. Wörmer and T. Möller, *Chem. Phys. Lett.*, 1991, **179**, 243–246.
93 R. Karnbach, M. Joppien and T. Möller, *J. Chim. Phys.*, 1995, **92**, 499–520.